

Type Ia supernovae

Stéphane Blondin,^{a,b}

^aAix Marseille Univ, CNRS, CNES, LAM, Marseille, France

^bEuropean Southern Observatory, Karl-Schwarzschild-Straße 2, Garching, D-85748, Germany

© 20xx Elsevier Ltd. All rights reserved.

Chapter Article tagline: update of previous edition,, reprint..

Glossary

Chandrasekhar mass (M_{Ch}) maximum mass for a white dwarf (WD) star; $M_{\text{Ch}} \approx 1.4 M_{\odot}$ for a cold, non-rotating, non-magnetic C-O WD.

Compton scattering in the context of SNe Ia, the scattering of γ -rays by electrons.

Deflagration-to-detonation transition (DDT) transition of the combustion mode from a subsonic deflagration to a supersonic detonation.

Double degenerate (DD) scenario progenitor channel for SNe Ia in which a WD merges or collides with another WD.

Electron degeneracy quantum-mechanical effect whereby a confined electron gas will exert a pressure even at zero temperature.

Electron fraction (Y_e) ratio of the number of electrons to nucleons (protons + neutrons) in a given chemical mixture.

Forbidden line spectral line resulting from the emission of a photon in an atomic transition with a very low transition probability.

Homologous expansion holds when the velocity of a fluid element is directly proportional to its radius, $v(r) \propto r$.

Iron-group elements (IGE) elements with atomic numbers in the range $Z = 21-28$ (i.e. scandium to nickel).

Intermediate-mass elements (IME) elements with atomic numbers in the range $Z = 11-20$ (i.e. sodium to calcium).

Local thermodynamic equilibrium (LTE) state of equilibrium between matter and radiation at the local temperature.

Metallicity abundance of all elements heavier than hydrogen and helium.

Nebular phase phase in the SN Ia evolution when the ejecta are transparent and the deposited energy is instantaneously re-emitted.

Nuclear statistical equilibrium (NSE) state of balance in nuclear reactions reached in explosive burning at high temperatures.

Opacity mass extinction coefficient specifying the energy fraction taken from a beam of photons due to absorption and scattering processes.

Optical depth measure of the level of transparency of a medium. Optically thick (thin) refers to an opaque (transparent) medium.

Radiative transfer generic term used to describe the theory of photon-matter interactions as radiation is transported through a medium.

Single degenerate (SD) scenario progenitor channel for SNe Ia in which a WD accretes material from a non-degenerate star.

Supernova (SN) energetic stellar explosion marking the end of the life of some stars.

Thermalization in SNe Ia, process by which γ -ray photons deposit their energy in the ejecta and are reprocessed into thermal radiation.

Type Ia supernova (SN Ia) supernova resulting from the thermonuclear disruption of a carbon-oxygen (C-O) white dwarf (WD) star.

UVOIR luminosity luminosity integrated over the full ultraviolet-optical-infrared range (i.e., excluding escaping high-energy radiation).

White dwarf (WD) star Compact and dense star marking the endpoint of the evolution of stars with initial masses $M \lesssim 8 M_{\odot}$.

Nomenclature

CE	common envelope
CSM	circumstellar material
DD	double degenerate
DDT	deflagration-to-detonation transition
DTD	delay-time distribution
EC	electron capture
HV	hypervelocity
HVF	high-velocity feature
IGE	iron-group elements
IME	intermediate-mass elements
LTE	local thermodynamic equilibrium
MS	main sequence
NSE	nuclear statistical equilibrium
SD	single degenerate
SN Ia	Type Ia supernova
UVOIR	ultraviolet(UV)-optical-infrared(IR)
WD	white dwarf

Abstract

Type Ia supernovae (SNe Ia) correspond to the thermonuclear explosion of a carbon-oxygen white dwarf (C-O WD) star in a binary system, triggered by the accretion of material from another star, or the merger/collision with a secondary WD. Their phenomenal luminosity — several billion times that of the sun — has motivated their use as cosmological distance indicators and led to the

2 Type Ia supernovae

discovery of the accelerated expansion of the universe. SNe Ia are also the main producers of iron and hence play a fundamental role in the chemical evolution of galaxies. While recent observations have confirmed the basic theoretical picture of an exploding C-O WD star whose luminosity is powered by the radioactive decay of ^{56}Ni , a number of uncertainties remain concerning the nature of the binary companion and the explosion mechanism. Several lines of evidence point towards the existence of multiple progenitor channels in order to explain the full range of the observed diversity. A complete physical understanding of these energetic stellar explosions remains a long-lasting goal of modern astrophysics.

Key points

- Almost all progenitor scenarios for SNe Ia involve a carbon-oxygen white dwarf star in a binary system, but vary in the nature of the binary companion (non-degenerate star vs. another WD) and the explosion mechanism or combustion mode.
- The energy input from the radioactive decay of ^{56}Ni synthesized in the explosion largely determines the luminosity evolution during the first 2–3 years. The spectroscopic evolution provides a time-dependent scan of the chemically-stratified ejecta, and provides important clues related to its composition and expansion dynamics.
- Most SNe Ia form a relatively homogeneous class, albeit with variations in their peak luminosity and spectroscopic properties. There are however events displaying peculiar light curves and spectra, and this observed diversity could indicate the existence of multiple progenitor channels.
- While explosion models have different ejecta structures and levels of asymmetry, the predicted observational signatures are often similar and the modeling uncertainties still too large to make firm associations between individual SNe Ia and specific progenitor scenarios, except in a few rare cases. Long considered to be the most likely scenario, the explosion of near-Chandrasekhar-mass WDs still faces fundamental challenges and currently favored models involve pairs of sub- M_{Ch} WDs.
- Future surveys will discover several hundreds of SNe Ia each night, mostly for cosmological studies. However, detailed observations of individual events, from the pre-explosion phases to several years after, and covering the full electromagnetic spectrum (and soon gravitational waves), remain invaluable to constrain the mechanism(s) by which WD stars explode.

1 Introduction

Stars with initial masses $M \lesssim 8 M_{\odot}$ evolve to become compact and dense objects known as white dwarfs (WD). Isolated WDs slowly cool by radiating away their residual thermal energy on timescales that can exceed the present age of the universe. However, a carbon-oxygen (C-O) WD in a close binary system can accrete mass from a non-WD star, or merge/collide with another WD, resulting in a runaway thermonuclear fusion reaction chain that can unbind the entire star.

Such stellar explosions, known as Type Ia supernovae (hereafter SNe Ia), are among the most energetic in the universe, with typical explosion energies of the order of 10^{44} J. Their luminosity reaches a typical peak value of $L_{\text{peak}} \approx 10^{36} \text{ J s}^{-1}$ (or $\sim 3 \times 10^9 L_{\odot}$), which is equivalent to a sizable 20-30% of the total luminosity of our own galaxy. For this reason, SNe Ia are visible out to very large distances, corresponding to a time when the universe was less than one fifth of its present age, only ~ 2 Gyr after the Big Bang (Pierel et al., 2024). Moreover, the realization that the light curves of SNe Ia could be used to accurately calibrate their peak brightness motivated the use of these events as distance indicators on cosmological scales. This unique property allowed astronomers to use SNe Ia as direct probes of the dynamical history of the universe, and led to the discovery of its accelerated expansion.

Type Ia SNe are also of great astrophysical interest in their own right. As the main producers of iron in the universe ($\sim 2/3$ of the iron content in our galaxy today; Dwek 2016), SNe Ia are key players in the chemical evolution of galaxies. They inject a significant amount of kinetic energy and turbulence into the interstellar medium, serving as a trigger for star formation and driving galaxy-scale winds. As an endpoint of binary stellar evolution for low-mass stars, SNe Ia require an understanding of mass transfer and accretion onto compact objects, and double-WD systems are predicted to be the dominating source of background gravitational-wave radiation for the future Laser Interferometer Space Antenna (LISA). As is the case for other types of SNe, their long-lived remnants, some of which are visible in our own galaxy (SN 1006, Tycho's SN 1572, Kepler's SN 1604), are thought to be sites for cosmic-ray acceleration. Last, their explosion mechanism involves all the complexity and richness of turbulent and shock-driven combustion, and is therefore of interest beyond the astrophysical community. Yet, despite decades of observational and theoretical efforts, the exact nature of the progenitors and explosion mechanisms of SNe Ia remains an unsolved question to date.

In this chapter, we will first review the basic underlying physical model for SNe Ia and characterize their observational properties (Section 2). In Section 3 we give an overview of the main progenitor and explosion scenarios invoked to explain the diversity of the SN Ia class. In Section 4, we discuss paths for future progress in the understanding of the SN Ia phenomenon, both from an observational and theoretical perspective. Concluding remarks follow in Section 5.

2 Basic physical picture and observational properties

2.1 A carbon-oxygen white dwarf progenitor

Unlike other types of supernovae resulting from the core collapse in massive stars, there are no direct detections of the exploding star in an SN Ia event, and only limited evidence related to the nature of the binary companion (with firm non-detections of a giant companion in some cases). One therefore has to rely on indirect clues. One such clue is the absence of lines due to hydrogen or helium — the two most

abundant elements in the universe — in their spectra around maximum light. This, combined with the occurrence of SNe Ia in early-type galaxies dominated by old stellar populations, suggests SNe Ia are associated with an evolved progenitor. Last, the rapid evolution of the light curve ($\lesssim 20$ days from explosion to peak luminosity, followed by a rapid decline on a similar timescale), provides indirect evidence for a relatively compact progenitor (further evidence is discussed in Section 2.3.1). Put together, a carbon-oxygen WD star emerges as the only viable progenitor for SNe Ia.

Carbon-oxygen white dwarfs are the endpoint of the evolution of stars with initial masses $2 \lesssim M \lesssim 8 M_{\odot}$ ¹. Such stars reach core temperatures for the fusion of helium into carbon and oxygen as they evolve off the main sequence (MS) to become red giant stars. As the C-O core contracts, the gravitational potential energy released is sufficient to eject the star's envelope, and its density is such ($\sim 10^9 \text{ kg m}^{-3}$ on average) that the electrons are degenerate and can be relativistic: It is this degeneracy pressure of the electrons that counteracts the inward pull of gravity, maintaining the star in hydrostatic equilibrium, before the temperature threshold for carbon fusion is reached in the core. Under these conditions, a WD star has a maximum mass it can sustain, known as the Chandrasekhar mass (Chandrasekhar, 1931), whose value depends only on composition, and is approximately $M_{\text{Ch}} \approx 1.44 M_{\odot}$ for a cold, non-rotating, non-magnetic C-O WD star in the ultra-relativistic limit:

$$M_{\text{Ch}} = 0.197 \left(\frac{hc}{G} \right)^{\frac{3}{2}} \frac{1}{(\mu_e m_{\text{H}})} \approx 1.44 M_{\odot} \quad \text{for } \mu_e = 2, \quad (1)$$

where μ_e is the average molecular weight per electron ($\mu_e = 2$ for a fully ionized C-O mixture) and m_{H} is the mass of the hydrogen atom (the other fundamental constants have their usual meaning).

The existence of a maximum mass for WDs could explain why the majority of SNe Ia appear to constitute a relatively homogeneous class, at least by astronomical standards. Since the majority of C-O WDs are born with an initial mass well below $1 M_{\odot}$ (Kepler et al., 2007), this implies that they must accrete mass from a binary companion, or merge with another WD in order to reach $\sim 1.4 M_{\odot}$ ². However, the SN Ia class is significantly more diverse than was originally thought, and currently-favored models for the explosion involve WDs well below the Chandrasekhar mass (sub- M_{Ch}).

2.2 Basic explosion physics

In the classical model of Hoyle and Fowler (1960), as the WD approaches M_{Ch} , the core temperature (a few times 10^8 K) and density ($\gtrsim 2 \times 10^{12} \text{ kg m}^{-3}$) is sufficient to initiate carbon fusion. Each subsequent increase in the WD mass via accretion leads to a contraction of the core and an increase in temperature via compressional heating, which in turn results in a rapid increase in the nuclear reaction rate and a further rise in temperature. In a normal (non-degenerate) star, this feedback process is self-regulated via an increase in the gas thermal pressure which leads to an expansion of the star and a drop of the core temperature. Under purely degenerate conditions, however, the pressure is independent of temperature. The above cycle is then self-sustained and the nuclear fusion reactions may undergo a runaway process.

The increase in temperature is in part compensated via various cooling mechanisms (neutrino emission, thermal conduction, and convection). The WD will eventually expand when the thermal pressure becomes comparable to the electron degeneracy pressure. Convective motions can initially evacuate the surplus nuclear energy and regulate nuclear reactions³, but it is not efficient enough to prevent the formation of a large temperature gradient and the initiation of a deflagration via thermal conduction. The flame is born, and a thermonuclear runaway follows. Although this basic physical picture differs somewhat in lower-mass (sub- M_{Ch}) WDs, the explosion as a SN Ia always proceeds via a runaway thermonuclear C-O fusion.

The fusion of $\sim 1.4 M_{\odot}$ of an equal mixture of ^{12}C and ^{16}O into iron-group elements (IGEs) releases enough nuclear energy ($E_{\text{nuc}} \approx 2 \times 10^{44} \text{ J}$)⁴, which is enough to unbind the WD and accelerate the ejecta to typical expansion velocities of the order of 10^7 m s^{-1} , as inferred from the blueshifted absorption in spectral lines:

$$E_{\text{nuc}} \approx -E_{\text{b}} + E_{\text{kin}}, \quad (2)$$

where the gravitational binding energy (negative by convention) $E_{\text{b}} \approx -5 \times 10^{43} \text{ J}$ for a non-rotating M_{Ch} WD, and the total kinetic energy $E_{\text{kin}} \lesssim 1.5 \times 10^{44} \text{ J}$.

A few seconds after the onset of the explosion, the expansion follows a self-similar regime referred to as homologous expansion (see glossary). The expansion is such that adiabatic losses cause the WD to cool very quickly: within one day after explosion, the WD has expanded from a Earth-sized object ($R \approx 10^6 \text{ m}$) to an ejecta whose size is similar to that of the solar system ($R \approx 10^{12} \text{ m}$). This would normally cause the maximum temperature in the ejecta to drop from $\sim 10^9 \text{ K}$ at a few seconds post explosion (at which point all nuclear reactions have ceased) to a few 1000 K at one day, and to room temperature ($\sim 300 \text{ K}$) by 10 days in the absence of an additional source of energy. SNe Ia would thus escape detection were it not for the abundant production of a radioactive isotope of nickel, ^{56}Ni (Colgate and McKee, 1969). This isotope decays to ^{56}Co via electron capture (EC) and finally to ^{56}Fe via EC or positron decay (β^+), emitting γ -rays and

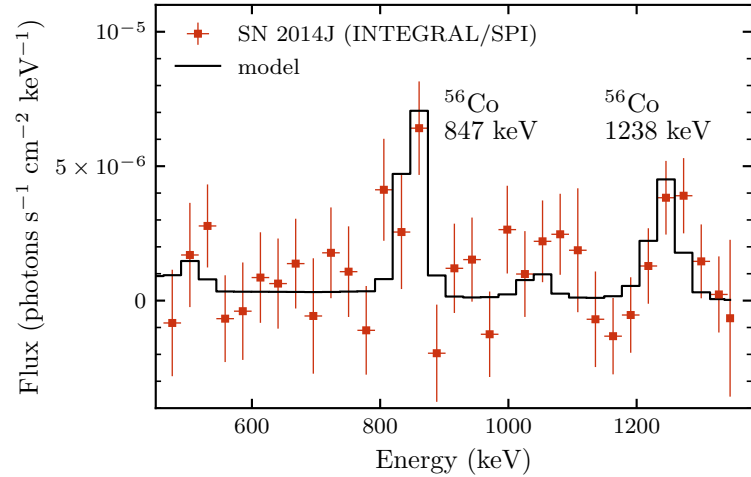
¹The lower limit of $\sim 2 M_{\odot}$ corresponds to the maximum initial mass of a star that can lead to the formation of a helium WD in a close binary system. For single stars this lower limit is slightly below $1 M_{\odot}$ (i.e. our sun will eventually evolve to become a C-O WD).

²There are however models for SNe Ia resulting from isolated WDs, such as the fission-based model of Horowitz and Caplan (2021).

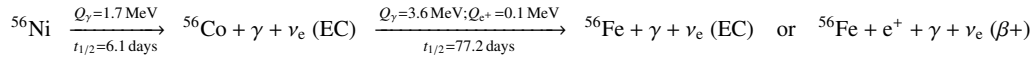
³This is known as the simmering phase and can last for several thousands of years.

⁴In cgs units this is equal to $2 \times 10^{51} \text{ erg}$, where 10^{51} erg is sometimes referred to as one Bethe (in honor of Hans Bethe), or one foe (fifty-one ergs).

Fig. 1: Detection of the 847 keV and 1238 keV (1 keV $\approx 1.6 \times 10^{-16}$ J) γ -ray decay lines of ^{56}Co in INTEGRAL/SPI observations of the nearby Type Ia SN 2014J (data from Churazov et al. 2014). This is the only direct detection to date of γ -rays in a SN Ia event.



positrons whose energy is deposited in the ejecta on timescales where adiabatic losses (proportional to the differential change in volume, dV) become less important:



where Q_{γ, e^+} corresponds to the average energy per decay (1 MeV $\approx 1.6 \times 10^{-13}$ J) emitted in γ -rays and positrons, respectively, and $t_{1/2}$ is the isotope's half-life. Only relatively recently has there been direct observational evidence of this decay-powered luminosity in SNe Ia, through the detection of γ -ray lines from ^{56}Co in the nearest SN Ia observed in the last 50 years, SN 2014J (Fig. 1).

The products of nuclear burning largely depend on the local fuel density. At sufficiently high densities, carbon fusion proceeds all the way to the iron peak, and nuclear statistical equilibrium (NSE) is established for temperatures $\gtrsim 5 \times 10^9$ K. These conditions ensure that the nucleosynthesis products do not depend on individual reaction rates, but only depend on the peak temperature, density, and electron fraction Y_e . This latter quantity is set by the initial metallicity of the WD (Y_e is lower for higher metallicity) and further modified by electron captures during the high-density pre-explosion simmering phase and during the explosion itself in M_{Ch} events. The final abundances in regions where NSE is reached are determined during the freeze-out phase, during which free particles reassemble into nuclei on timescales inversely proportional to the density. In lower-density regions, carbon fusion does not proceed to the iron peak as the silicon-burning process is incomplete. These are the regions where most of the intermediate-mass elements (IMEs) are synthesized.

The dependence of the nuclear burning products on density implies that the mass of the exploding WD also affects the integrated yields, as M_{Ch} WDs have larger central densities ($\rho_c \gtrsim 10^{12}$ kg m $^{-3}$) compared to lower-mass, sub- M_{Ch} WDs ($\rho_c \lesssim 10^{11}$ kg m $^{-3}$). As a result, burning in NSE produces more heavier neutron-rich stable isotopes (e.g. ^{54}Fe and ^{58}Ni) in M_{Ch} explosions compared to sub- M_{Ch} explosions for a given initial metallicity. The stable nickel abundance can thus be used in principle to distinguish M_{Ch} from sub- M_{Ch} explosions (e.g. Flörs et al., 2020). This also applies to manganese, whose solar abundance can only be explained if a significant fraction of SNe Ia achieve the high-density burning conditions met in M_{Ch} progenitors (Seitenzahl et al., 2013a).

Together with the chemical stratification inferred from the time evolution of SN Ia spectra (see next section), we can already highlight three basic ingredients for a successful SN Ia model (see box below). The final ingredient of course is to allow for some diversity to match what is seen in nature. One possible model that satisfies these requirements is illustrated in Fig. 2.

Three basic ingredients for a successful SN Ia model

1. **Explosion energy:** of the order of 10^{44} J to unbind the WD and accelerate the ejecta to characteristic velocities of the order of 10^7 m s $^{-1}$. This implies the WD must be (almost) entirely burnt to release sufficient nuclear energy from fusion of C-O into heavier elements.
Note: some explosion models (e.g. pure deflagrations) result in too low an explosion energy to completely unbind the WD, in which case a bound remnant is left behind. Such models have been found to be a good candidate for low-luminosity Type Iax events.
2. **Nucleosynthesis:** A ^{56}Ni yield in the range 0.1–1.0 M_\odot (to power the light curve) + several 0.1 M_\odot of IMEs (to match the spectra) + some stable IGE isotopes (^{58}Ni , ^{54}Fe) + possible traces of unburnt C-O. This requires thermonuclear burning at a large range of densities.
3. **Chemical stratification:** stable IGEs + ^{56}Ni near the center and IMEs in the outer layers. This requires a large (exponentially decreasing) density gradient and weak large-scale mixing during the explosive phase.
Note: the inner ejecta of violent merger models are dominated by the ashes of the incompletely burned secondary WD (O, Ne, Mg), and pure deflagration models predict significant amounts of unburnt C-O material as a result of large-scale mixing during the explosion.

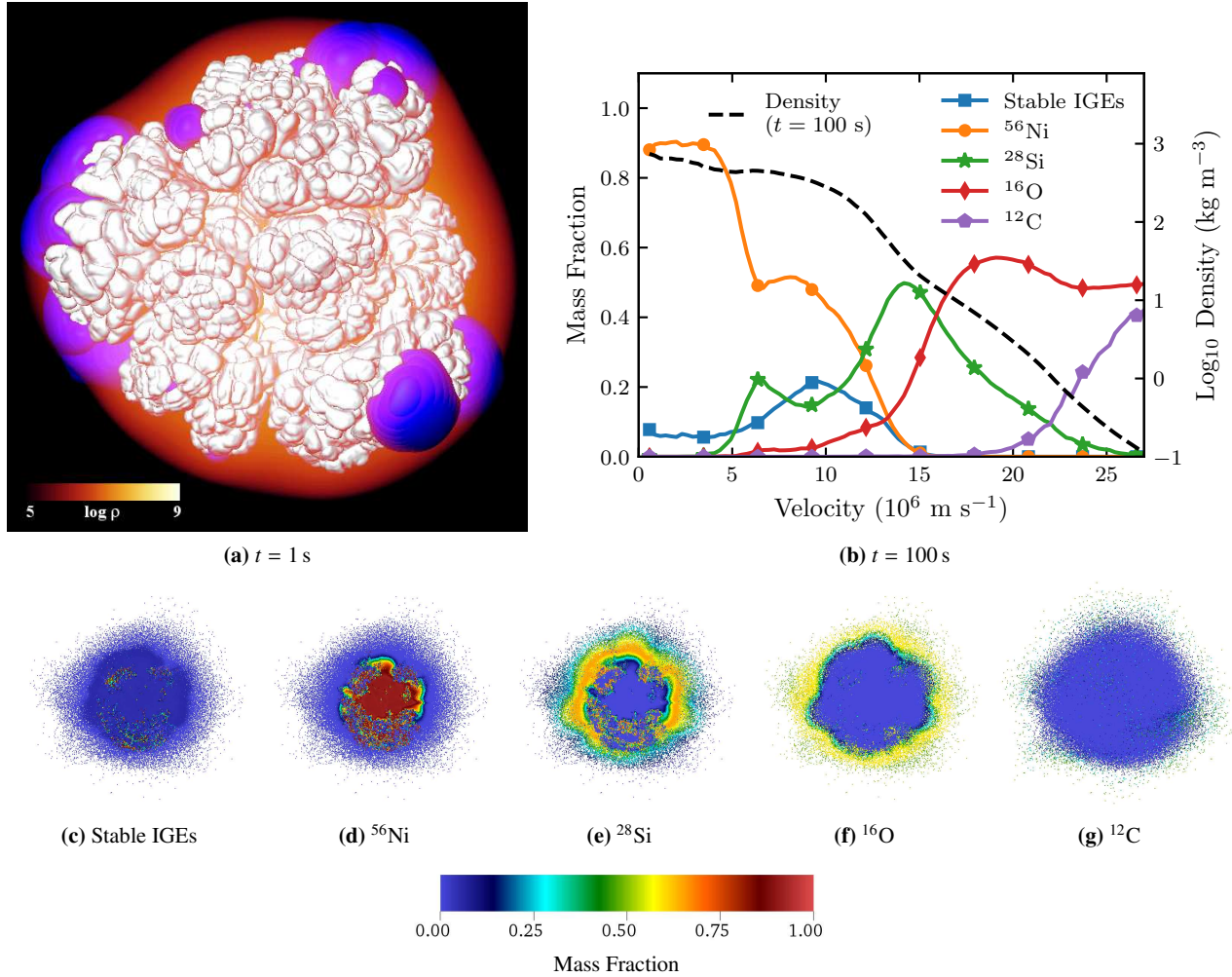


Fig. 2: Example of a 3D M_{Ch} delayed-detonation model (N100; Seitenzahl et al. 2013b). (a) Density (in $\text{g cm}^{-3} = 10^3 \text{ kg m}^{-3}$; orange color scale), deflagration plumes (white), and detonation front (blue) at $t = 1$ s post explosion. (b) Spherically averaged density (dashed line) and composition profiles for representative isotopes (solid lines) at $t = 100$ s post explosion. The 2D-projected distribution of each isotope is shown in the bottom row in panels (c)–(g). The graphics shown in panels (a) and (c)–(g) are reproduced with permission from Seitenzahl et al. (2013b, their Figs. 2 and 4).

2.3 Luminosity and spectroscopic evolution

We illustrate the evolution of the UVOIR luminosity for a SN Ia model in Fig. 3. As the ejecta expands, the radiation emerges from deeper ejecta layers⁵, offering a time-dependent scan of its chemical structure (Fig. 4). In what follows we will discuss four main phases of the evolution over the first few months post explosion, focusing on normal SN Ia events.

2.3.1 Early evolution

Although ^{56}Ni decay is the main driver for the luminosity evolution, the early luminosity of SNe Ia can be affected by other factors. Most SN Ia explosion models involve combustion driven by a strong supersonic shock (i.e. a detonation). A predicted observational consequence is a UV-optical flash of radiation resulting from the shock-heated stellar envelope and lasting $\lesssim 1$ h, whose luminosity $L_{\text{shock}} \approx 10^{32} \text{ J s}^{-1}$ (i.e. four orders of magnitude lower than the peak luminosity; Rabinak et al. 2012) has never been observed⁶. This early-time flash can in principle be followed by a dark phase during which ^{56}Ni decay photons are still trapped within the ejecta (estimated to last ~ 1 day in the case of SN 2011fe; Mazzali et al. 2014).

During the first few days that follow, the γ -ray photons emitted in the ^{56}Ni decay chain are completely thermalized by Compton scattering

⁵At least in a Lagrangian sense, as these deeper layers are expanding at several 10^6 m s^{-1} .

⁶However, it is the non-detection of this signature in the nearby Type Ia SN 2011fe that enabled to place a strong constraint on the progenitor radius $R_* \lesssim 0.02 R_{\odot}$ (Bloom et al., 2012). Also note that an even earlier, shorter-lived signature is expected in X-rays, when the shock breaks out from the stellar envelope.

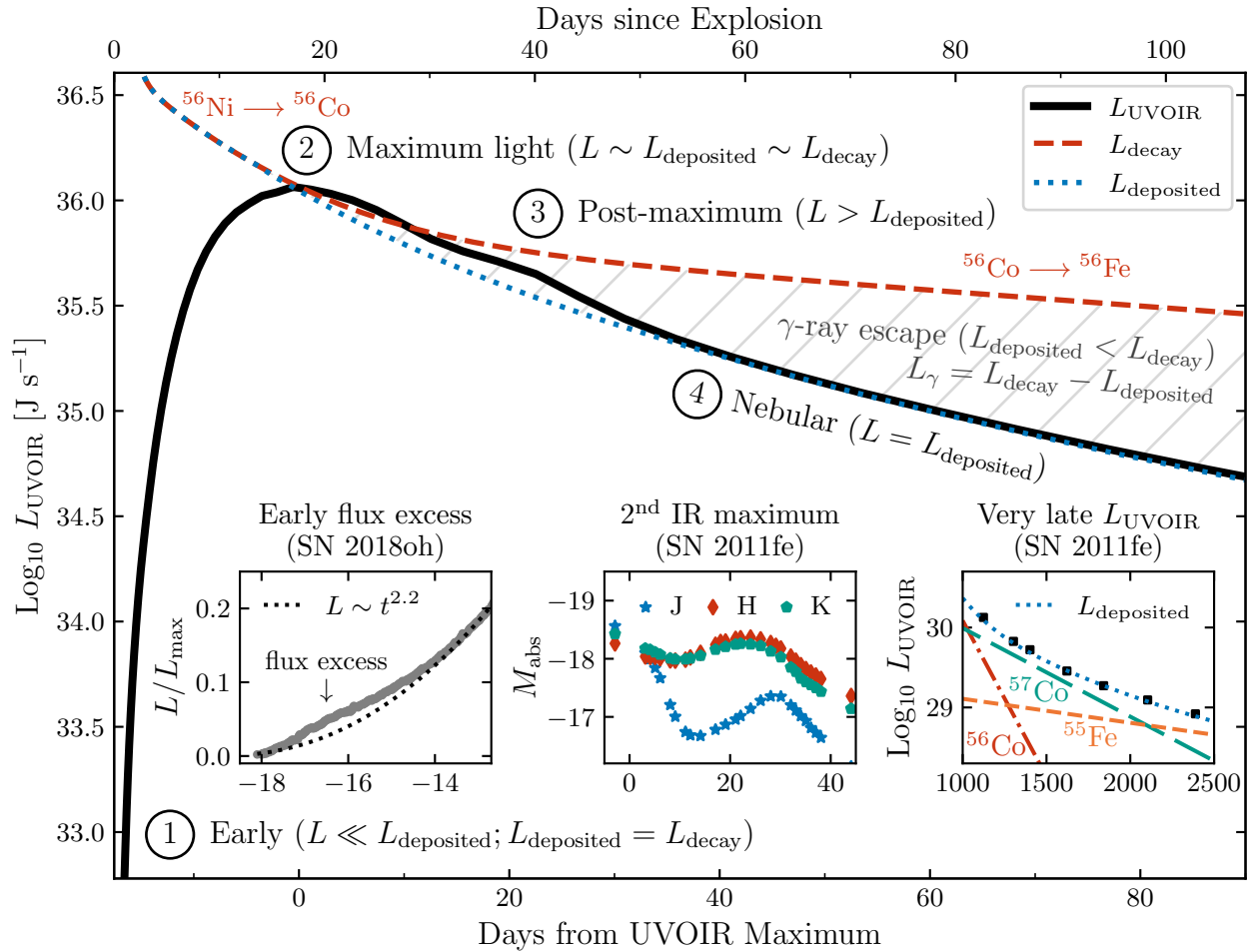


Fig. 3: Luminosity evolution for a SN Ia model with $\sim 0.5 M_{\odot}$ of ^{56}Ni (black solid line; DDC15 model of Blondin et al. 2015). The dashed and dotted lines show the decay luminosity and the deposited decay power, respectively. The hatched area highlights the increasing γ -ray escape past maximum light. The insets give examples of early flux excess (left; data from Dimitriadis et al. 2019), the secondary near-IR maximum (middle; data from Matheson et al. 2012), and the contribution of additional decay chains to the luminosity at very late times (right; data from Tucker et al. 2022). The axis in each case corresponds to days from maximum light.

off free electrons. Due to the high initial optical depth, this thermal radiation diffuses over a time scale significantly larger than the time elapsed since the explosion, such that the initial luminosity is very low. As the ejecta expands, the photon escape time becomes less than the characteristic expansion time, and the luminosity increases. This initial increase is often modeled as a power law in time, $L(t) \propto t^{\alpha}$, where $\alpha = 2$ matches well the early light curve of SN 2011fe (Nugent et al., 2011). However, both theoretical predictions and observations find significant deviations from $\alpha = 2$ (Piro and Nakar, 2014; Firth et al., 2015). Moreover, an early flux excess has been observed in several SNe Ia (left inset in Fig. 3), which could result from the interaction with a binary companion or circumstellar material (CSM), or from the presence of ^{56}Ni in the outer regions of the ejecta.

The optical spectra at these times are dominated by Doppler-broadened lines of ions from IMEs synthesized in the explosion (e.g. Si II, S II, Ca II etc.), as well as lines from unburnt carbon (first spectrum in Fig. 4). The characteristic P-Cygni profile shape of these lines displays a prominent blueshifted absorption that is used to infer the expansion velocity of the corresponding ion. In particular, high-velocity features (HVF) are routinely found in lines of Ca II and Si II (see insets in Fig. 4). These HVFs are sometimes associated with a spectropolarimetric signature, indicating an asymmetric distribution of the emitting material (e.g. Kasen et al., 2003).

2.3.2 Peak luminosity (maximum light)

The initial increase in luminosity is counterbalanced by the exponentially decreasing decay power, which causes a maximum in the light curve. At this time, the UVOIR luminosity is comparable (but not physically equivalent) to the decay power injected in the inner ejecta layers: this is known as Arnett’s rule (Arnett, 1979), and can be formally expressed as $L_{\text{UVOIR}}(t_{\text{peak}}) \approx \alpha L_{\text{decay}}(t_{\text{peak}})$, with $\alpha \approx 1$. Several studies have found this rule to be accurate to within 10–20% (e.g. Blondin et al., 2013). The maximum-light spectra are still dominated by lines from IMEs, and early-time signatures of unburnt carbon have usually disappeared by then.

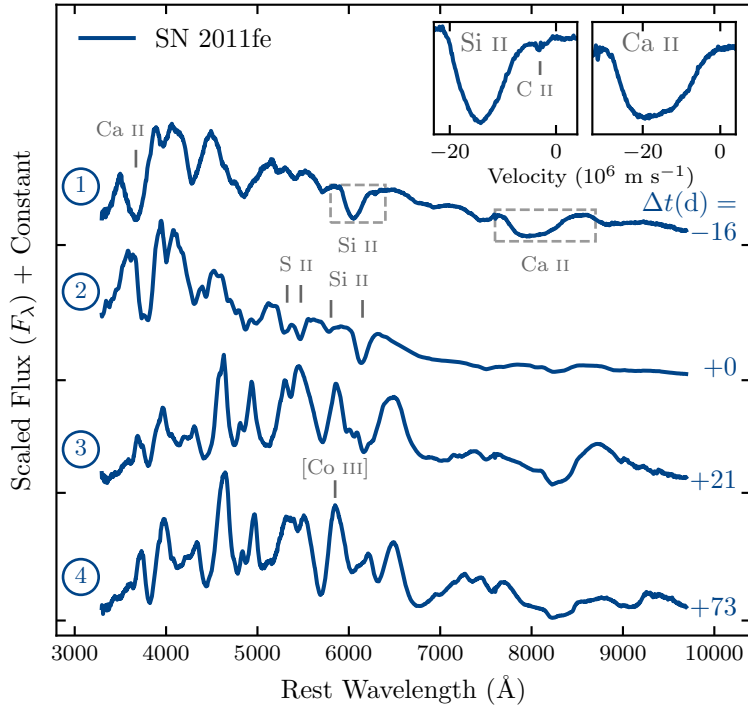


Fig. 4: Spectroscopic evolution of the Type Ia SN 2011fe over the first ~ 100 days post explosion (data from Pereira et al. 2013). The right labels give the spectral phase in days from maximum light, and the circled numbers on the left correspond to the phases highlighted in Fig. 3. The tickmarks on the Y-axis give the zero-flux level of each spectrum. A few key spectroscopic features are highlighted in gray. The insets show examples of high-velocity features at early times in the Si II 6355 Å and Ca II near-IR triplet line profiles. A small absorption due to C II 6580 Å (i.e. unburnt carbon) can also be seen in the left inset.

2.3.3 Post-maximum evolution

Two notable phenomena occur after the peak in luminosity. First, the rate of energy actually deposited in the ejecta (dotted curve in Fig. 3) becomes an increasingly smaller fraction of the radioactive decay power (mainly from ^{56}Co decay at this time; dashed curve). This is due to the increase in the mean free path of γ -ray photons, an ever-increasing fraction of which manages to escape directly from the ejecta without interaction⁷. Second, the luminosity exceeds the energy deposition rate during ~ 30 days, which corresponds to the time needed to radiate the energy stored at previous times. Around 40 days post explosion, we even observe a slight inflection in the light curve: radiative processes lead to a cooling of the ejecta, including emission by forbidden lines (such as [Co III] 5888 Å; Dessart et al. 2014). This releases a significant amount of radiative energy ($\Delta E_{\text{rad}} \approx a_R \Delta T^4 \Delta V$, where a_R is the radiation constant), of the order of 10^{35} J s^{-1} . To this inflection in the evolution of the UVOIR luminosity corresponds a second peak in the light curves in the near-IR bands (*JHK*; see middle inset in Fig. 3).

More luminous SNe Ia decline more slowly past maximum light in several photometric bands (i.e. their light curves are broader) compared to lower-luminosity events: this is known as the width-luminosity relation (Phillips, 1993). It results from the faster evolution to redder colors in lower-luminosity events around maximum light, which causes a more rapid decline in the blue optical bands (Kasen and Woosley, 2007).

2.3.4 Late-time evolution: the nebular phase

Finally, from ~ 50 days after the explosion onward, the ejecta becomes almost completely transparent, and the luminosity equals (and is physically equivalent to) the rate of decay energy deposition in the ejecta, an increasing fraction of which comes from positrons from ^{56}Co decay⁸: this is known as the nebular phase. One can further show that the time-weighted integral of the UVOIR luminosity is equal to that of the deposited decay power by this time (Katz et al., 2013), a property that can be used to infer the ^{56}Ni mass from observations without relying on the less accurate Arnett rule:

$$\int_0^t t' L_{\text{UVOIR}}(t') dt' = \int_0^t t' L_{\text{dep}}(t') dt' \quad \text{for } t \gg t_{\text{peak}}. \quad (3)$$

The nebular spectra now probe the innermost ejecta and reflect the iron-group dominated composition there (Fig. 5). The most prominent lines are due to forbidden transitions of Fe and Co, with some evidence of weak lines from nickel. The overlying IMEs, visible at earlier phases, also contribute to the cooling. Since all of the ^{56}Ni synthesized in the explosion has long decayed by this time, all the nickel left in the ejecta is made up of stable isotopes (mainly ^{58}Ni). As noted in Section 2.2, the abundance of these stable isotopes can in principle be

⁷The characteristic γ -ray escape time scales with the square root of the total ejecta mass (Jeffery, 1999), and has led several authors to conclude that a significant fraction of SNe Ia result from sub- M_{Ch} progenitors (Stritzinger et al., 2006; Scalzo et al., 2014; Wygoda et al., 2019).

⁸Other radioactive decay chains become important at even later times, such as ^{57}Co ($t_{1/2} \approx 272$ days) and ^{55}Fe ($t_{1/2} \approx 1000$ days), both confirmed observationally in the nearby SN 2011fe (see right inset in Fig. 3).

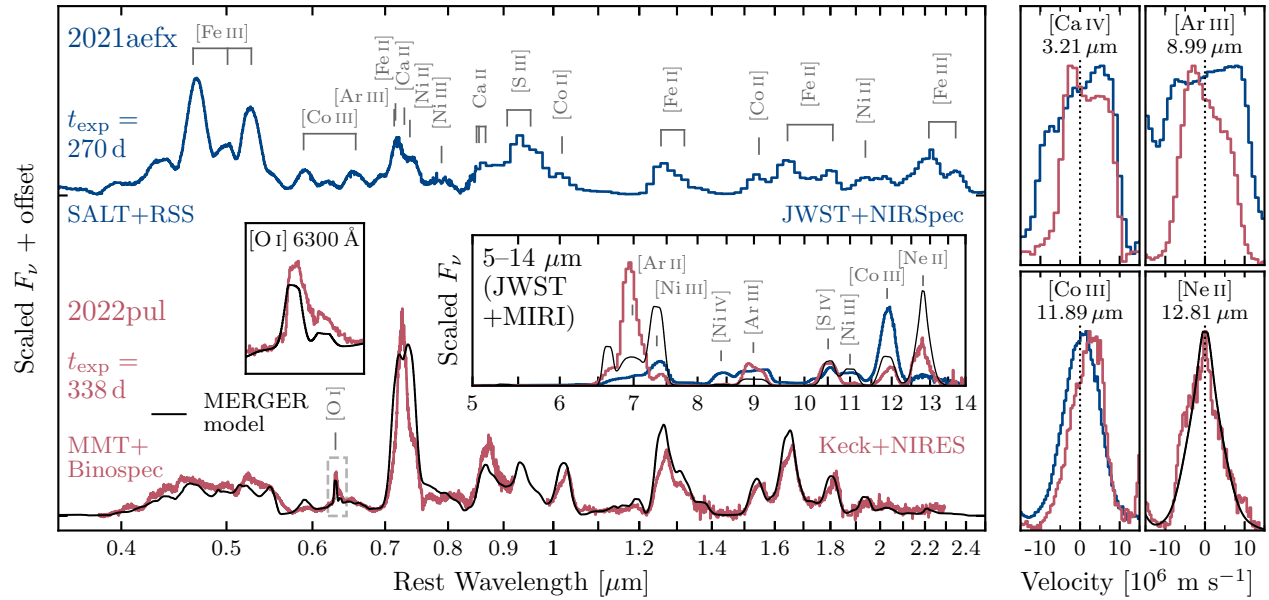


Fig. 5: Left panel: Nebular spectra of SN 2021aefx at 270 days post explosion (top) and of SN 2022pul at 338 days post explosion (bottom). The SN 2022pul spectrum is compared to a violent merger model, which correctly predicts a narrow [O I] 6300 Å doublet (solid line; see also left inset). Right panels: Comparison of mid-IR line profiles in both spectra, normalized to their peak intensity. Lines in this range are more isolated and reveal variations in morphology (boxy vs. peaked), as well as kinematic offsets of several 10^6 m s^{-1} . The mid-IR spectrum of SN 2022pul shows a prominent line due to [Ne II] 12.81 μm , which is characteristic of the violent merger of two WDs (Kwok et al., 2024).

used to constrain the mass of the exploding WD.

The forbidden lines in nebular SN Ia spectra are optically thin and hence only visible in emission. The morphology of their profiles can be used to constrain the chemical distribution and ejecta geometry (right panels in Fig. 5). For instance, several SNe Ia display velocity shifts in their nebular line profiles (i.e. the lines are not centered on their rest wavelength), that could result from an off-center explosion (Maeda et al., 2010). Other events display a horn-like double-peaked morphology, consistent with predictions of WD-WD collision models (Dong et al., 2015). More recently, the James Webb Space Telescope (JWST) has paved the way for systematic studies of SNe Ia in the mid-IR spectral range. Observations of one event, SN 2022pul, have revealed the presence of a strong line due to [Ne II] 12.8 μm , presented as a smoking-gun signature of the violent merger of two WDs (see MERGER model spectrum in Fig. 5).

2.4 Observational diversity

The basic physical picture outlined above applies to the bulk of the SN Ia population, and can accommodate part of the observed diversity (in rise time, peak luminosity, post-maximum decline rate, color evolution, and spectroscopic properties; see Fig. 6), some of which could be simply due to viewing-angle effects in an asymmetric explosion. At the high-luminosity end are the 91T-like SNe Ia that resemble the prototypical SN 1991T, characterized by a higher ionization and abundance of IGEs in the outer layers, and sometimes associated with CSM interaction (see Phillips et al. 2024 for a recent review). At the low-luminosity end, 91bg-like SNe Ia (resembling the prototypical SN 1991bg) are characterized by a deep Ti II/Cr II absorption trough in their early-time optical spectra, redder colors at early times, and the absence of a secondary maximum in their near-IR light curves. Some authors have explained this diversity as a continuous sequence in temperature/ionization related to the ^{56}Ni yield (e.g. Nugent et al., 1995).

There are however peculiar events that possibly constitute distinct sub-classes, and these are sometimes collectively referred to as “thermonuclear supernovae” or “white dwarf supernovae” (see Taubenberger 2017 for a review). Of these, we highlight super-luminous SNe Ia (e.g. SN 2009dc) sometimes associated with the explosion of rapidly-rotating super-massive WDs (Yoon and Langer, 2005)⁹, which could also form via the merger of a sub- M_{Ch} WD and the C-O core of an asymptotic giant branch star inside a common envelope (core-degenerate scenario; Kashi and Soker 2011); SNe Ia that display strong narrow hydrogen lines resulting from interaction with a dense CSM (Ia-CSM; e.g. SN 2002ic); low-luminosity events with low ejecta velocities that resemble SN 2002cx (referred to as Type Iax SNe; see Jha 2017 for a review); and low-luminosity events similar to SN 2002es with a slow post-maximum decline in luminosity (i.e. contrary to the width-luminosity relation). Example light curves and maximum-light spectra of these events are shown in Fig. 6.

⁹Often referred to as “super- M_{Ch} ” SNe Ia since their mass exceeds $\sim 1.4 M_{\odot}$, although this canonical value only applies to a non-rotating WD, which is not the case here.

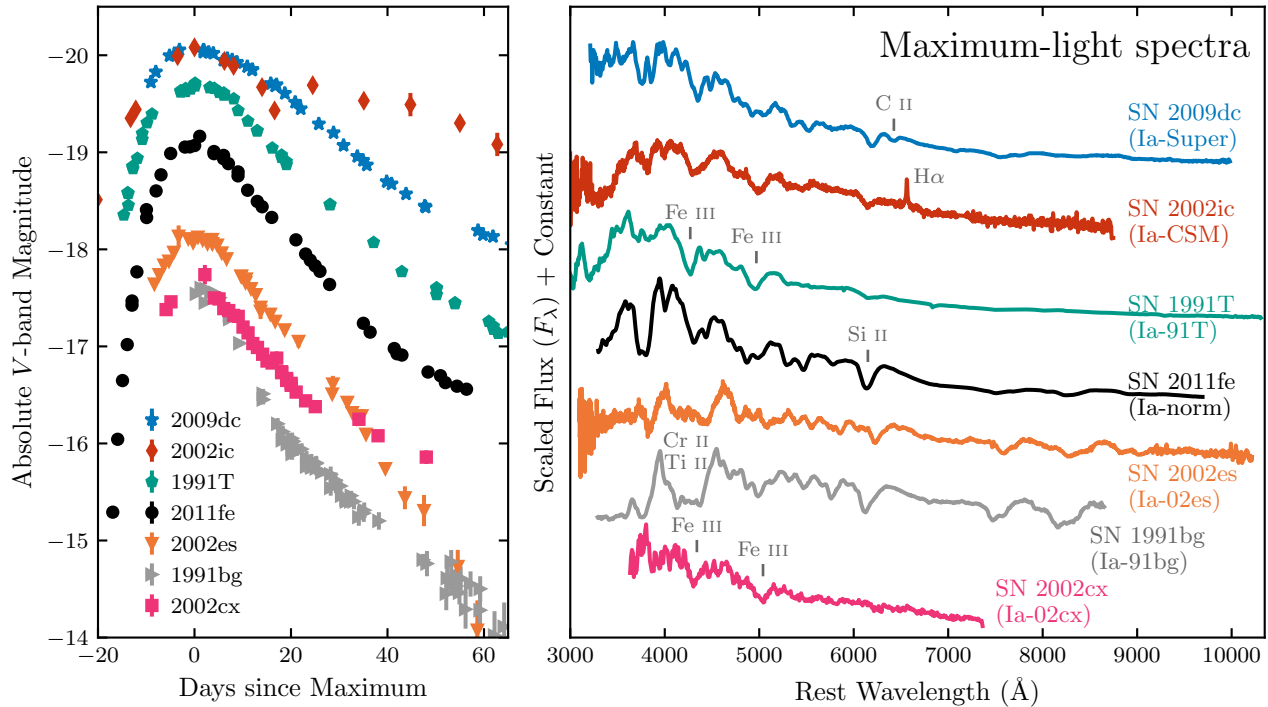


Fig. 6: The observational diversity of SNe Ia, both in terms of their peak luminosity and light-curve shape (here in the V band; left) and their spectroscopic properties (here around maximum light; right). Data sources: SN 2009dc (Taubenberger et al., 2011), SN 2002ic (Hamuy et al., 2003; Wood-Vasey et al., 2004), SN 1991T (Phillips et al., 1992; Lira et al., 1998; Altavilla et al., 2004), SN 2011fe (Richmond and Smith, 2012; Pereira et al., 2013), SN 2002es (Hicken et al., 2009; Ganeshalingam et al., 2012), SN 1991bg (Filippenko et al., 1992; Leibundgut et al., 1993; Turatto et al., 1996), SN 2002cx (Li et al., 2003).

2.5 Modeling challenges

Before presenting possible progenitor scenarios and explosion mechanisms in Section 3, we first comment on some of the theoretical and numerical challenges associated with modeling SNe Ia.

2.5.1 Thermonuclear burning fronts

The first of these concerns modeling thermonuclear burning fronts (see Röpke 2017 for a review). Combustion fronts can propagate via two modes: subsonic deflagrations (which propagate via thermal conduction and are accelerated via interaction with turbulence) and supersonic detonations (which propagate via a strong shock). A deflagration can also transition to a detonation via a deflagration-to-detonation transition (DDT), relevant for M_{Ch} SN Ia models (see Section 3.1), but which poses a major challenge even in terrestrial combustion experiments (Poludnenko et al., 2019).

Because of the steep dependence of nuclear reaction rates on temperature, combustion fronts are confined to a thin layer that can be well below 10^{-3} m, which is more than nine orders of magnitude smaller than the WD radius ($\gtrsim 10^6$ m). The modeling of deflagrations requires knowledge of microphysical processes that cannot be resolved in multi-dimensional simulations, even with advanced numerical methods such as adaptive mesh refinement. While such knowledge is not necessary when modeling detonation fronts, these display a multi-dimensional cellular pattern whose inner structure is also left unresolved. In both cases, the combustion front must either be artificially broadened to match the resolution of the numerical grid, or treated as a sharp discontinuity (level-set approach; as seen in Fig. 2) whose propagation speed is determined a priori as opposed to computed self consistently.

2.5.2 Explosive nucleosynthesis

Computing accurate yields in SN Ia explosion simulations is also faced with a resolution problem, as the reaction length scales vary by several orders of magnitude (see Seitenzahl and Townsley 2017 for a review). The number of isotopes involved in the nuclear reactions relevant to carbon burning is also prohibitively large to be included in multi-dimensional hydrodynamical simulations of the explosion (200–300 isotopes in typical SN Ia reaction networks). The strategy is then to consider smaller networks coupled to the hydrodynamics that match the nuclear energy release – which serves for instance to propagate the detonation front – predicted using larger networks, and then compute the accurate nucleosynthesis as part of a post-processing step (using Lagrangian tracer particles; e.g. Travaglio et al. 2004).

2.5.3 Radiative transfer

To predict the observable signatures from a given explosion model, one needs to model the interaction of the radiation with the rapidly-expanding ejecta, i.e. solve a radiative-transfer (RT) problem. There are various approaches to this, from solving the RT equation along rays to following photon packets in a Monte Carlo experiment. Most RT simulations are initiated at ~ 1 day after the explosion, at which point the ejecta are in homologous expansion and one can choose to ignore the hydrodynamical part of the problem. Up until the nebular phase, however, time-dependent effects should be taken into account since there is a delay between the injection of energy from the ^{56}Ni decay chain and the resulting escape of thermalized photons from the SN ejecta. Non-local energy deposition by γ -rays and non-thermal effects resulting from fast electrons generated in Compton scatterings of these γ -rays also need to be treated self consistently.

Furthermore, RT simulations in the context of SNe Ia are complicated due to the nature of the opacity (e.g. Pinto and Eastman, 2000). The dominance of atomic lines (bound-bound transitions), which both absorb and scatter incoming photons, has the effect of decoupling the radiation field from the local thermodynamical conditions of the gas (temperature and electron density). One then needs to solve numerous rate equations to compute the populations n_i (number density, m^{-3}) of each atomic level i for each ion considered in the solution. The IGEs that dominate the composition of SN Ia ejecta have several thousands of individual levels and millions of bound-bound transitions between them. Solving the complete set of rate equations comes at a huge computational cost, even in 1D, which becomes prohibitively large in 3D.

One strategy is to treat the entire problem assuming spherical symmetry (1D), but this overlooks the inversion of the chemical stratification between the stable IGEs and ^{56}Ni -rich layers as predicted in 3D models of the explosion (for M_{Ch} DDT models). Another approach is to start with spherical averages of a 3D explosion model, but this then artificially mixes together regions burnt at a wide range of densities and hence leads to chemical inconsistencies (e.g. Pakmor et al., 2024). Last, treating the entire problem (hydrodynamics + RT) in 3D requires the sacrifice of physical consistency (e.g. in the treatment of ionization) to save computational costs. Even in 1D, starting with the same initial ejecta model does not guarantee that different codes will yield the same results (Blondin et al., 2022a).

3 Progenitor scenarios and explosion mechanisms

There are several viable progenitor scenarios for SNe Ia, with specific explosion mechanisms associated with each. For a long time, the explosion of a near- M_{Ch} WD was considered the most likely candidate, at least from a theoretical standpoint, but recent years have witnessed a regained interest in models involving sub- M_{Ch} WD pairs, in particular violent mergers and double-detonation models. Different models, however, can yield similar observable signatures, as the outcome of the explosion in terms of ejecta dynamics and composition are sometimes weakly sensitive to the initial state of the WD or the details of the nuclear burning¹⁰. That said, a few observed SNe Ia have displayed smoking-gun signatures associated with a particular scenario. In what follows we review the main explosion models considered by the community today. The different progenitor channels associated with each model are schematically illustrated in Fig. 7, and Table 1 summarizes some of their most salient features.

3.1 The classical Chandrasekhar-mass model, or single-degenerate (SD) scenario

Long considered the standard model for SNe Ia, this model involves a WD that accretes material from a non-degenerate binary companion until its mass approaches M_{Ch} . Here, the combustion must first proceed as a deflagration and then transition to a detonation via the DDT mechanism (Khokhlov, 1991). Indeed, pure deflagrations result in weak explosions that sometimes fail to completely unbind the WD (such models have been proposed for Type Iax events), while pure detonations are ruled out as they burn the entire WD to IGEs, with too little IMEs needed to reproduce the early-time spectra¹¹. Various flavors of this delayed-detonation model exist, such as gravitationally-confined detonations or pulsationally-reversed detonations. The key requirement is that the WD is pre-expanded during the deflagration phase before the detonation burns the remainder of the WD at lower densities, producing IMEs in sufficient amounts.

The advantages of the SD scenario is that it naturally provides the correct conditions to ignite carbon fusion in the WD core, in addition to a physical basis (namely the M_{Ch} limit) for the observed homogeneity of a large fraction of the SN Ia sample. Some nucleosynthesis arguments (such as the abundance of manganese in the solar neighborhood; see Section 2.2) point towards the need for a significant contribution of M_{Ch} progenitors to the SN Ia population. Chandrasekhar-mass delayed-detonation models have also been successful at reproducing the observed light curves and spectra of normal SNe Ia, although the range in ^{56}Ni yield needed to reproduce the observed range in peak luminosity requires a somewhat artificial tuning of the density at which the DDT occurs.

But this long favored model has several essential shortcomings. Starting with stellar evolution, growing a WD via accretion to M_{Ch} requires a fine tuning of the accretion rate to values of the order of $10^{-7} M_{\odot} \text{yr}^{-1}$ (Nomoto et al., 1984), and the predicted rates for the SD channel are too low by at least one order of magnitude compared to the observed SN Ia rate – although these results are subject to uncertainties related for instance to the common envelope (CE) phase of the evolution, critical to forming close interacting binary systems. The SD scenario is also difficult to reconcile with the long delay times of a few Gyrs between WD formation and explosion as inferred from delay-time distributions (DTD; see Maoz et al. 2014). Last, some nucleosynthesis constraints instead impose an upper limit on the fraction of SNe Ia resulting from M_{Ch} progenitors (e.g. Bravo et al., 2022).

The lack of a direct and unambiguous detection of the companion, even in the favorable case of the nearby SN 2011fe (e.g. Tucker and Shappee, 2024), as well as in SN Ia remnants in our galaxy or in the Large Magellanic Cloud (e.g. Kerzendorf et al., 2018), is problematic.

¹⁰P. Höflich coined the term “stellar amnesia” to describe this lack of sensitivity to the initial conditions (e.g. Höflich, 2006).

¹¹Pure detonations of sub- M_{Ch} WDs however do produce the correct mix of IGEs and IMEs since their initial density is lower compared to M_{Ch} WDs.

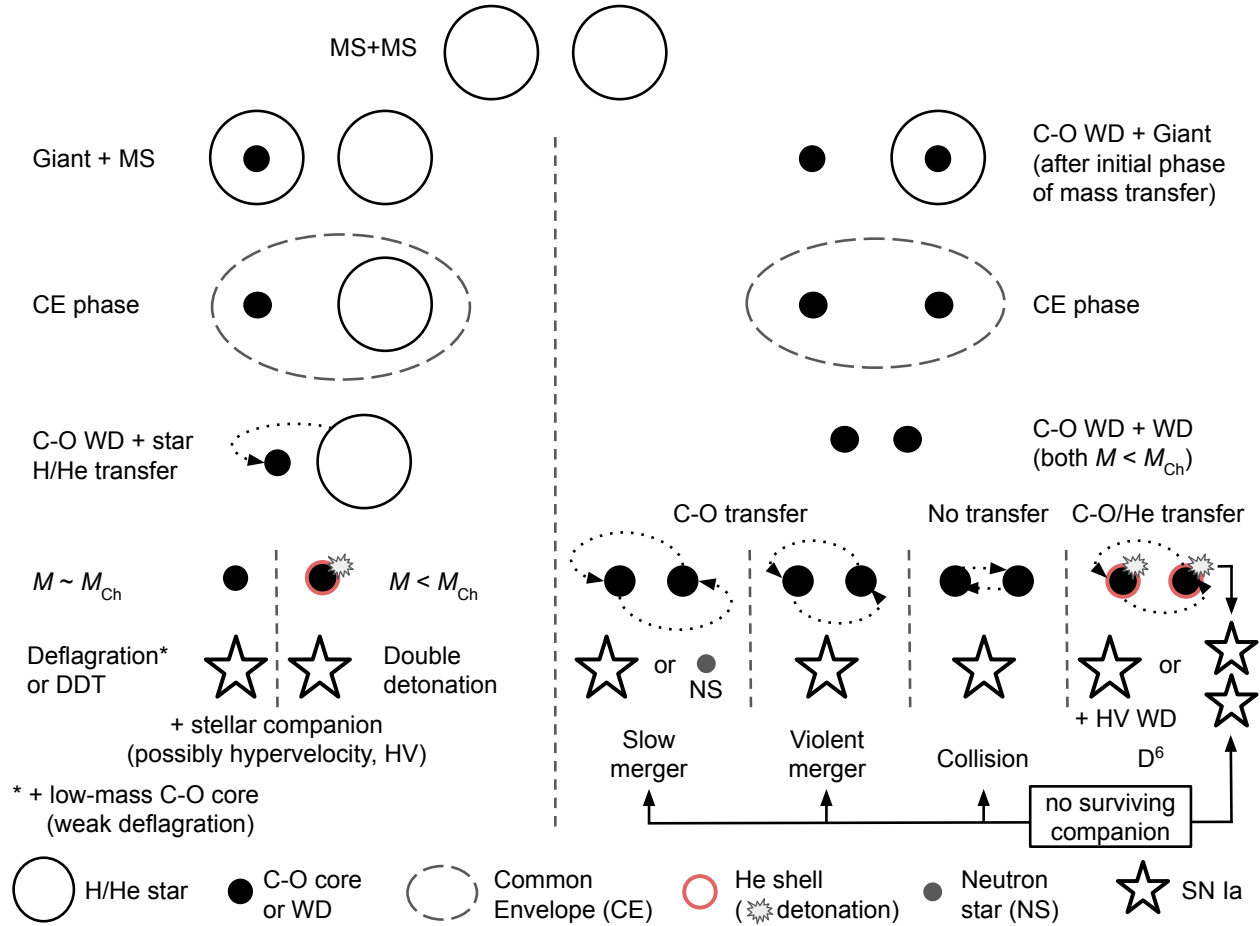


Fig. 7: Schematic view of the six SN Ia progenitor channels presented in this chapter, starting with a main sequence (MS) binary system and proceeding through different evolutionary stages and final outcomes (each separated by a dashed vertical line).

Indirect detections include interaction of the rapidly-expanding ejecta with the companion¹², leading to an early-time signature at UV-blue wavelengths (Kasen, 2010). Such signatures have been seen in several SNe Ia but none have been unambiguously associated with interaction with a companion. Likewise, H-rich material stripped from the companion as it is overtaken by the SN ejecta should result in narrow hydrogen lines in the nebular spectra, with only one firm detection so far (Prieto et al., 2020). Pre-SN mass loss via winds from the companion, in addition to left-over material from the accretion phase, should lead to a complex CSM with which the SN ejecta interacts, resulting in radio signatures only detected in one event so far (SN 2020eyj; Kool et al. 2023). This event also displayed spectroscopic signatures of interaction with a He-rich CSM from a helium star companion. An X-ray signature is also expected in the SD scenario, either during the pre-explosion phase as a supersoft X-ray source, or resulting from CSM interaction. This has only been detected in one event at nebular times (Bochenek et al., 2018), and no detection has been reported even in the case of Ia-CSM events (Dwarkadas, 2024). The pre-SN wind is also expected to carve out a low-density cavity in the surrounding CSM, which has not been convincingly detected in SN Ia remnants; these instead appear to be expanding into a uniform medium (Badenes et al., 2007).

3.2 Double-detonations in sub-Chandrasekhar-mass WDs with stable mass transfer

Pure detonations of sub- M_{Ch} WDs provide a viable alternative to the aforementioned M_{Ch} SD scenario. One immediate advantage is the abundance of lower-mass WDs which could account for the observed SN Ia rate. Second, the range of typical WD masses considered in such models (0.8–1.1 M_{\odot}) results in a range of density profiles and hence a range in ^{56}Ni yields which naturally explains the observed diversity in peak luminosity. In particular, the rapidly-evolving light curves of low-luminosity 91bg-like SNe Ia seemingly require a sub- M_{Ch} ejecta (Blondin et al., 2017).

¹²Except in the “spin up-spin down” scenario, where the WD must first rid itself of the excess angular momentum gained via accretion before exploding, during which time the companion continues to shed its envelope, shrinking considerably in size (Justham, 2011).

Table 1: Basic characteristics of progenitor scenarios for SNe Ia.

Scenario	Combustion Mode ^a	M_{WD} (primary)	Companion	Surviving Companion ^b	Early Interaction	Nebular Lines ^c
Single WD progenitor systems						
Single degenerate	delayed-DET	$\sim M_{\text{Ch}}$	MS/Giant or He star	HV star or slow stripped Giant ^d (+ low-mass C/O core ^e)	companion and CSM	narrow H α + velocity shifts ^f
	DEF					narrow [O I]
Double detonation	DET (He+C)	sub- M_{Ch}	He star	HV star	companion and CSM	...
Double WD progenitor systems						
Slow WD merger (Double-degenerate)	DET	sub- M_{Ch} or $\sim M_{\text{Ch}}$	sub- M_{Ch} WD	none or NS ^g	C-O envelope	...
Violent WD merger	DET	sub- M_{Ch}	sub- M_{Ch} WD	none	...	[Ne II] + narrow [O I]
D ⁶ (one explosion)	DET (He+C)	sub- M_{Ch}	sub- M_{Ch} WD (C-O or He)	HV WD	...	velocity shifts
D ⁶ (two explosions)				none	...	velocity shifts + double-peaked
WD collision	DET	sub- M_{Ch}	sub- M_{Ch} WD	none or HV 3 rd star ^h	...	double-peaked

^a delayed-DET = delayed detonation; DEF = pure deflagration; DET = pure detonation.

^b HV = hypervelocity.

^c we only report on peculiar spectroscopic signatures.

^d a giant donor would survive the explosion partially stripped of its outer H/He-rich envelope, and be ejected from the system at a lower velocity compared to less massive companions.

^e for weak deflagrations that fail to completely unbind the WD.

^f nebular line shifts are expected in an explosion ignited off-center.

^g such slow mergers can lead to an accretion-induced collapse to a neutron star and hence no SN Ia event.

^h for triple systems consisting of a double-WD binary and a third low-mass star.

In order to explode, sub- M_{Ch} WDs require the formation of a helium shell around the C-O core, via accretion of H-rich material (which burns to helium on the WD surface) or He-rich material from a donor star. Here we consider cases where the mass transfer is stable. This helium shell must somehow detonate near its base, driving a powerful shock wave into the WD, leading to a secondary detonation of the C-O core. Initial models considered a relatively massive helium shell ($\lesssim 0.2 M_{\odot}$), whose detonation produces copious amounts of ^{56}Ni and other IGEs that are in conflict with the early-time spectra. Subsequent theoretical investigations showed that less massive helium shells (a few $0.01 M_{\odot}$) were able to detonate and produce a successful secondary explosion while leaving little IGE-rich material in the outer ejecta (e.g. [Fink et al., 2010](#)).

There is a common misconception that the explosion of sub- M_{Ch} WDs produces no stable isotopes of nickel. Despite the lower densities involved in the burning ($\lesssim 10^{11} \text{ kg m}^{-3}$), stable ^{58}Ni is produced in NSE in sub- M_{Ch} explosions, albeit at a lower abundance compared to M_{Ch} models at a given metallicity. The strength of the nebular forbidden lines of nickel is highly sensitive to the ionization state of the Ni-rich layers, such that abundance determinations are uncertain ([Blondin et al., 2022b](#)). Moreover, there is no unambiguous correspondence between the stable nickel mass and the mass of the exploding WD, since some M_{Ch} models (e.g. gravitationally-confined detonations) predict similar stable IGE yields as sub- M_{Ch} models. Nonetheless, [Flörs et al. \(2020\)](#) attempted to estimate the stable Ni/Fe ratio from late-time spectra, and concluded that the majority of the SNe Ia in their sample were not only consistent with sub- M_{Ch} explosions, but also inconsistent with the predictions from standard M_{Ch} DDT models.

3.3 Slow mergers or the classical double-degenerate (DD) scenario

In this scenario, two unequal-mass sub- M_{Ch} C-O WDs in a close binary system (whose total mass exceeds M_{Ch}) slowly spiral in via emission of gravitational waves ([Webbink, 1984](#); [Iben and Tutukov, 1984](#)). The less massive (secondary) WD is disrupted and forms a hot envelope surrounded by an accretion disk around the more massive (primary) WD. The rapid accretion of C-O-rich material onto the primary WD ensures an efficient increase in mass (possibly approaching M_{Ch}), at which point the conditions for carbon ignition are reached in the core — as in the classical M_{Ch} scenario. The explosion will thus occur within a massive C-O envelope, resulting in an interaction at early times that

could explain some super-luminous SNe Ia (e.g. [Taubenberger et al., 2013](#)). However, the spectroscopic properties of such an interaction have not yet been thoroughly investigated.

This scenario naturally explains the absence of hydrogen and helium lines in the spectra of SNe Ia, as well as the lack of any firm detection of a non-degenerate companion star¹³. Moreover, the loss of angular momentum via gravitational-wave radiation results in a power-law DTD $\propto t^{-1}$ consistent with observations ([Maoz and Mannucci, 2012](#)). The predicted rates of DD systems are also closer to the observed SN Ia rate, although it has been argued that mergers of sub- M_{Ch} WDs whose combined mass is less than M_{Ch} must also contribute ([van Kerkwijk et al., 2010](#)). However, surveys devoted to the discovery of close double-WD systems have only discovered a handful of candidates that will merge within a Hubble time, and only two systems with a combined mass either consistent with M_{Ch} ([Geier et al., 2007](#)) or slightly exceeding M_{Ch} ([Pelisoli et al., 2021](#)).

One major drawback of the DD scenario is a result of the predicted high accretion rate onto the primary WD. It is thought to lead to an off-center ignition of carbon and the formation of a high-mass O-Ne WD, with a subsequent accretion-induced collapse to a neutron star and hence no SN Ia event (e.g. [Shen et al., 2012](#)).

3.4 Violent mergers

In contrast to the slow WD mergers discussed above, carbon ignition in violent WD mergers occurs in the immediate precursor phase or during the merger event itself. The first simulations showed that merging two near-equal-mass $\sim 0.9 M_{\odot}$ WDs would lead to violent accretion of the less massive WD onto the primary, and a hotspot would form at the interface between the direct accretion stream and the C-O core of the more massive WD, possibly resulting in carbon ignition and a thermonuclear runaway ([Pakmor et al., 2010](#)). Since the exploding WD is significantly sub- M_{Ch} , the amount of ^{56}Ni synthesized in the explosion is rather small and only consistent with low-luminosity SNe Ia. However, the larger ejecta mass results in longer diffusion timescales, hence the predicted light curves are broader than for classical 91bg-like events, although possibly compatible with peculiar low-luminosity events such as SN 2010lp ([Kromer et al., 2013](#)). The secondary WD is only partially burned shortly after the explosion, and its oxygen-dominated ejecta expands inside that of the primary WD, which could explain the presence of narrow [O I] lines in nebular spectra of these sub-luminous events ([Kromer et al., 2016](#)).

Later studies considered unequal-mass WD systems with a more massive primary WD ($\sim 1.1 M_{\odot}$), resulting in ^{56}Ni yields compatible with a normal SN Ia event ([Pakmor et al., 2012](#)). As in the low-luminosity case above, the inner ejecta is dominated by the ashes of the partially-burnt secondary WD, which consist mostly of oxygen but also some neon. A strong forbidden line in the mid-IR range due to [Ne II] $12.8 \mu\text{m}$ was indeed predicted to emerge in nebular spectra of this violent merger model ([Blondin et al., 2023](#)), which was detected soon after and for the first time in a JWST spectrum of the Type Ia SN 2022pul ([Kwok et al. 2024](#); see Fig. 5).

While a promising scenario for SNe Ia, it is unclear whether the hotspot resulting from the direct-impact accretion stream actually leads to a detonation, although longer-term spiral instabilities may provide the necessary ignition conditions ([Kashyap et al., 2015](#)). Also, the predicted level of asymmetry in the ejecta can be fairly high, in contradiction with the low polarization levels commonly observed in SNe Ia ([Bulla et al., 2016](#)) and with the spherical morphology of SN Ia remnants.

3.5 Double detonations in double-WD systems with dynamically unstable mass transfer (D⁶ scenario)

The initial configuration for this explosion scenario is similar to that for the violent mergers discussed above, and both result from a dynamically unstable mass transfer. However, the explosion here is triggered by the detonation of a thin helium layer on the primary WD (either present initially or accreted from the secondary WD) – as opposed to direct carbon ignition in its core. This initial detonation then leads to a secondary detonation of the C-O core, as in the classical double-detonation scenario (Section 3.2). Such explosions are referred to as helium-ignited violent mergers ([Pakmor et al., 2013](#)) or more poetically as dynamically driven double degenerate double detonations (D⁶; [Shen et al. 2018b](#)).

One important observational consequence compared to violent mergers is that the secondary WD can survive the explosion and be ejected from the system as a hypervelocity (HV) WD with peculiar chemical composition. Several HV WDs have in fact been detected by the *Gaia* satellite, confirming the viability of this scenario, although in too low numbers to explain the majority of SNe Ia ([Shen et al., 2018a](#)). However, if a thin helium shell is also present on the secondary WD, the impact of the rapidly-expanding ejecta from the primary can lead to its detonation and a subsequent double-detonation explosion of the secondary, i.e. a quadruple-detonation event ([Pakmor et al., 2022](#)). The predicted delay of a few seconds between both explosions leads to the expansion of the secondary WD's ejecta inside that of the primary, leading to possible late-time signatures of asymmetries and peculiar chemical profiles that could help distinguish quadruple detonations from cases where the secondary WD survives the explosion.

3.6 Collisions

There is a non-negligible probability for two WDs in dense stellar environments (such as globular clusters or galactic nuclei) to collide head-on with one another ([Benz et al., 1989](#)). Such collisions are however expected to be rare, even when taking into account Kozai-Lidov resonances induced by a third low-mass star orbiting the inner WD binary (e.g. [Katz and Dong, 2012](#)). Numerical simulations of head-on collisions of WD pairs with varying masses and impact parameters have been able to produce successful explosions with ^{56}Ni yields that match the observed range in peak luminosity. A bimodal ^{56}Ni distribution is often expected in such models, resulting in double-peaked emission lines of cobalt and iron at late times that have been detected in a few nebular SN Ia spectra ([Dong et al., 2015](#)). It is still unclear

¹³This statement also applies to all the other double-WD scenarios discussed in the following sections (3.4–3.6).

however whether these features are a smoking-gun signature for this scenario, as double-peaked profiles could also result from quadruple detonations in the D^6 scenario discussed above.

4 Ongoing and future developments

Here we mention a few ongoing and future efforts to better understand the nature of SNe Ia, both from observational and theoretical/modeling perspectives.

4.1 Observations

There already exists a plethora of high-quality photometric and spectroscopic data for SNe Ia collected over several decades. That said, more recent high-cadence surveys – such as the Asteroid Terrestrial-impact Last Alert System (ATLAS; [Tonry et al. 2018](#)) or the Zwicky Transient Facility (ZTF; [Bellm et al. 2019](#)) – have enabled the systematic discovery of SNe Ia within a few days from the explosion. Studies of the earliest phases of the evolution places important constraints on the presence of a (massive) binary companion or CSM, or on the presence of ^{56}Ni in the outer ejecta (see Section 2.3.1).

The upcoming Vera Rubin Observatory, with its ten-year Legacy Survey of Space and Time (LSST), will discover and monitor over a million SNe Ia starting in 2025. The observing cadence, however, will result in relatively sparsely-sampled light curves, and spectroscopic follow-up is not included in the survey design and will be limited to a small fraction of the total sample. Rubin/LSST will also discover over a hundred strongly-lensed SNe Ia out to redshifts $z \lesssim 1$ that are strongly lensed by a foreground galaxy ([Arendse et al., 2024](#)), producing multiple images of the SN that appear at different times. By detecting the first appearing SN image, one can use the predicted time delays between the multiple images to catch the SN right at the moment of its next appearance, and hence access the first hours/days of its evolution ([Suyu et al., 2020](#)). Moreover, the rest-frame UV radiation of these high-redshift events can be observed with ground-based facilities at optical wavelengths, providing complementary diagnostics to high-cadence surveys targeting nearby events.

The recent launch of JWST has enabled the systematic study of SNe Ia at mid-IR wavelengths – such data only existed for a handful of events before then. The first late-time spectra of SNe Ia obtained with JWST revealed for the first time the $2.5\text{--}5\ \mu\text{m}$ range for these events, as well as the detection of the $[\text{Ne II}]$ $12.8\ \mu\text{m}$ line in one event, as predicted by violent merger models (see Fig. 5). The *Euclid* satellite, although not designed for transient surveys, could be used to complement the high-redshift SN Ia sample of Rubin/LSST for cosmological studies at near-IR wavelengths ([Bailey et al., 2023](#)). The future Nancy Grace Roman Space Telescope (NGRST), on the other hand, will carry out a dedicated near-IR survey of a few thousand SNe Ia ([Hounsell et al., 2018](#))¹⁴.

At higher frequencies, the X-ray satellite XRISM (launched in September 2023), and hopefully succeeded by ESA’s NewAthena mission in the late 2030’s, will carry out spatially-resolved spectroscopic studies of SN Ia remnants, thereby directly constraining the explosion energetics and ejecta chemical stratification. In the γ -ray regime, the Compton Spectrometer and Imager (COSI; planned launch in 2025) should be able to detect energetic photons resulting from the ^{44}Ti decay chain, whose abundance can be used to discriminate between different SN Ia explosion mechanisms (e.g. [Kosakowski et al., 2023](#)).

Last, the revolution wrought by the direct detection of gravitational waves has opened up a new channel for studying astronomical events, including SNe Ia. Double WD systems are expected to largely dominate over all other compact binaries detected by LISA in our galaxy ([Amaro-Seoane et al., 2023](#)), with an expected $\gtrsim 2000$ WD+WD systems with a primary mass exceeding $0.8 M_{\odot}$ that could explode as SNe Ia ([Korol et al. 2024](#) and private communication). LISA will also be able to detect WD+black hole binaries and test the scenario in which a WD is tidally stripped by an intermediate-mass ($< 10^5 M_{\odot}$) black hole ([Rosswog et al., 2009](#)).

4.2 Theory and Modeling

On the theoretical and modeling fronts, ongoing efforts are focused on stellar evolution, the hydrodynamics of the explosion and its coupling to the nucleosynthesis, and the radiative-transfer post-processing.

Concerning stellar evolution, 3D modeling of the common envelope phase of evolution is currently being undertaken to better understand how close binary systems can form. More accurate rate estimates for the M_{Ch} channel require a better understanding of accretion processes onto WDs that can result in a near- M_{Ch} progenitor, as well as of the pre-explosion simmering phase.

Numerical modeling of the explosion still suffers from insufficient resolution to properly model the combustion fronts in SNe Ia, although recent simulations have been able to resolve the detonation of a thin helium layer atop a C-O WD, with a grid-cell resolution of a few tens of meters only (F. Röpke, private communication). However, nucleosynthesis calculations still largely rely on post processing explosion simulations via tracer particles, where one would prefer a direct coupling of nuclear reaction networks to the hydrodynamics ([Bravo, 2020](#)). The predicted abundances of various isotopes are however only weakly sensitive to uncertainties in nuclear reaction rates ([Bravo and Martínez-Pinedo, 2012](#)). Last, terrestrial combustion experiments, in particular related to the DDT mechanism in unconfined media, can provide useful insights into the treatment of combustion fronts in simulations of the explosion ([Thomas et al., 2022](#)).

Radiative-transfer simulations still represent a major hurdle in connecting explosion models with observations (light curves and spectra). While a 3D treatment of the problem seems warranted, there is a trade-off to be made between the dimensionality and physical consistency or resolution of the simulation, and full time-dependent non-LTE simulations are currently lacking. One related major limitation concerns the availability of atomic data, whose accuracy can have a significant impact on spectroscopically determined abundances ([Blondin et al.,](#)

¹⁴This paper refers to the WFIRST project, since then rebaptized NGRST.

2023). Sophisticated numerical calculations are required to compute cross-sections for important atomic processes (e.g. photoionization, collisional excitation) as these cannot all be measured in the laboratory.

5 Concluding remarks

Much progress has been made in recent years towards a better understanding of the progenitors and explosion mechanisms of SNe Ia. High-cadence surveys have enabled to systematically discover new SNe Ia shortly after explosion and hence enable the study of their earliest phases, and JWST has given the community access to high-quality spectroscopic diagnostics in the mid-IR range. While future observational efforts will concentrate on gathering large samples of SNe Ia in the optical and near-IR ranges for cosmological studies, detailed studies of individual events (including radio, X-ray and γ -ray observations when possible) remain paramount for constraining key parameters of the explosion.

For a long time the single most-favored contender for explaining the bulk of SNe Ia, the M_{Ch} model is now invoked to explain more peculiar events, such as Type Iax SNe which are thought to result from pure deflagrations of M_{Ch} WDs. The recent emergence of double sub- M_{Ch} WD systems as the leading model for SNe Ia is an interesting reversal of the general consensus up to a decade ago, and testifies to the dynamism of this field of research. However, a word of caution is in order, as future observational findings and modeling efforts might be able to address some of the limitations of the M_{Ch} model. Likewise, future gravitational-wave detections of double-WD systems with LISA will be able to confirm or disprove the double-degenerate scenario as the dominant channel for SNe Ia. The jury is still out, and new ideas on how white dwarf stars explode will no doubt emerge in the coming years.

Acknowledgments

This chapter is dedicated to Tom Marsh (1961–2022), who introduced SB to the topic of Type Ia supernovae during his studies at the University of Southampton. We thank Eduardo Bravo, Robert Fisher, Bruno Leibundgut, and Ken Shen for carefully reading and providing detailed comments on a first draft of this chapter. We further acknowledge useful discussions with Luc Dessart, Roland Diehl, Valeriya Korol, Friedrich (Fritz) Röpke, Ivo Seitenzahl, with a special mention to Frank Timmes for inspiring the “Three basic ingredients for a successful SN Ia model” box in Section 2. We thank Stefano Benetti for providing the light-curve data for SN 2002ic used in Fig. 6 and Eugene Churazov for providing the SN 2014J data and model shown in Fig. 1. This work was supported by the Alexander von Humboldt foundation, and by the ‘Programme National de Physique Stellaire’ (PNPS) of CNRS/INSU co-funded by CEA and CNES.

See Also: Several chapters of the “Handbook of Supernovae” (Eds. A. W. Alsabti and P. Murdin), four of which are referenced in the present chapter, cover many aspects of SNe Ia in more depth, including their cosmological applications. Many explosion models for SNe Ia are publicly available online at the Heidelberg Supernova Model Archive (HESMA; <https://hesma.h-its.org>). The results of radiative-transfer simulations for supernova ejecta with the CMF-GEN code are accessible on Zenodo (<https://zenodo.org/communities/snrt>), and the results of a radiative-transfer code-comparison study are available on github (<https://github.com/sn-rad-trans/data1>; see Blondin et al. 2022a).

References

- Altavilla G, Fiorentino G, Marconi M, Musella I, Cappellaro E and et al. (2004), Apr. Cepheid calibration of Type Ia supernovae and the Hubble constant. *MNRAS* 349: 1344–1352. doi:10.1111/j.1365-2966.2004.07616.x. arXiv:astro-ph/0401273.
- Amaro-Seoane P, Andrews J, Arca Sedda M, Askar A, Baghi Q and et al. (2023), Mar. Astrophysics with the Laser Interferometer Space Antenna. *Living Reviews in Relativity* 26 (1), 2. doi:10.1007/s41114-022-00041-y. 2203.06016.
- Arendse N, Dhawan S, Sagués Carracedo A, Peiris HV, Goobar A and et al. (2024), Jul. Detecting strongly lensed type Ia supernovae with LSST. *MNRAS* 531 (3): 3509–3523. doi:10.1093/mnras/stae1356. 2312.04621.
- Arnett WD (1979), May. On the theory of Type I supernovae. *ApJL* 230: L37–L40. doi:10.1086/182957.
- Badenes C, Hughes JP, Bravo E and Langer N (2007), Jun. Are the Models for Type Ia Supernova Progenitors Consistent with the Properties of Supernova Remnants? *ApJ* 662 (1): 472–486. doi:10.1086/518022. astro-ph/0703321.
- Bailey AC, Vincenzi M, Scolnic D, Cuillandre JC, Rhodes J, Hook I, Peterson ER and Popovic B (2023), Oct. Type Ia supernova observations combining data from the Euclid mission and the Vera C. Rubin Observatory. *MNRAS* 524 (4): 5432–5441. doi:10.1093/mnras/stad2179. 2211.01206.
- Bellm EC, Kulkarni SR, Graham MJ, Dekany R, Smith RM and et al. (2019), Jan. The Zwicky Transient Facility: System Overview, Performance, and First Results. *PASP* 131 (995): 018002. doi:10.1088/1538-3873/aacbe. 1902.01932.
- Benz W, Hills JG and Thielemann FK (1989), Jul. Three-dimensional Hydrodynamical Simulations of Stellar Collision. II. White Dwarfs. *ApJ* 342: 986. doi:10.1086/167656.
- Blondin S, Dessart L, Hillier DJ and Khokhlov AM (2013), Mar. One-dimensional delayed-detonation models of Type Ia supernovae: confrontation to observations at bolometric maximum. *MNRAS* 429: 2127–2142. doi:10.1093/mnras/sts484. 1211.5892.
- Blondin S, Dessart L and Hillier DJ (2015), Apr. A one-dimensional Chandrasekhar-mass delayed-detonation model for the broad-lined Type Ia supernova 2002bo. *MNRAS* 448: 2766–2797. doi:10.1093/mnras/stv188. 1501.06583.
- Blondin S, Dessart L, Hillier DJ and Khokhlov AM (2017), Sep. Evidence for sub-Chandrasekhar-mass progenitors of Type Ia supernovae at the faint end of the width-luminosity relation. *MNRAS* 470: 157–165. doi:10.1093/mnras/stw2492. 1706.01901.

- Blondin S, Blinnikov S, Callan FP, Collins CE, Dessart L and et al. (2022a), Dec. StaNDaRT: a repository of standardised test models and outputs for supernova radiative transfer. *A&A* 668, A163. doi:10.1051/0004-6361/202244134. 2209.11671.
- Blondin S, Bravo E, Timmes FX, Dessart L and Hillier DJ (2022b), Apr. Stable nickel production in type Ia supernovae: A smoking gun for the progenitor mass? *A&A* 660, A96. doi:10.1051/0004-6361/202142323. 2109.13840.
- Blondin S, Dessart L, Hillier DJ, Ramsbottom CA and Storey PJ (2023), Jun. Nebular spectra from Type Ia supernova explosion models compared to JWST observations of SN 2021aefx. *arXiv e-prints*, arXiv:2306.07116doi:10.48550/arXiv.2306.07116. 2306.07116.
- Bloom JS, Kasen D, Shen KJ, Nugent PE, Butler NR and et al. (2012), Jan. A Compact Degenerate Primary-star Progenitor of SN 2011fe. *ApJL* 744, L17. doi:10.1088/2041-8205/744/2/L17. 1111.0966.
- Bochenek CD, Dwarkadas VV, Silverman JM, Fox OD, Chevalier RA, Smith N and Filippenko AV (2018), Jan. X-ray emission from SN 2012ca: A Type Ia-CSM supernova explosion in a dense surrounding medium. *MNRAS* 473 (1): 336–344. doi:10.1093/mnras/stx2029. 1708.07181.
- Bravo E (2020), May. The accuracy of post-processed nucleosynthesis. *MNRAS* 494 (2): 3037–3047. doi:10.1093/mnras/staa910. 2002.08486.
- Bravo E and Martínez-Pinedo G (2012), May. Sensitivity study of explosive nucleosynthesis in type Ia supernovae: Modification of individual thermonuclear reaction rates. *Phys. Rev. C* 85 (5), 055805. doi:10.1103/PhysRevC.85.055805. 1204.1981.
- Bravo E, Piersanti L, Blondin S, Domínguez I, Straniero O and Cristallo S (2022), Nov. Chandrasekhar-mass white dwarfs are the progenitors of a small fraction of Type Ia supernovae according to nucleosynthesis constraints. *MNRAS* 517 (1): L31–L35. doi:10.1093/mnras/slac103. 2209.04020.
- Bulla M, Sim SA, Pakmor R, Kromer M, Taubenberger S, Röpke FK, Hillebrandt W and Seitzzahl IR (2016), Jan. Type Ia supernovae from violent mergers of carbon-oxygen white dwarfs: polarization signatures. *MNRAS* 455 (1): 1060–1070. doi:10.1093/mnras/stv2402. 1510.04128.
- Chandrasekhar S (1931), Jul. The Maximum Mass of Ideal White Dwarfs. *ApJ* 74: 81–+.
- Churazov E, Sunyaev R, Isern J, Knödseder J, Jean P and et al. (2014), Aug. Cobalt-56 γ -ray emission lines from the type Ia supernova 2014J. *Nature* 512 (7515): 406–408. doi:10.1038/nature13672. 1405.3332.
- Colgate SA and McKee C (1969), Aug. Early Supernova Luminosity. *ApJ* 157: 623. doi:10.1086/150102.
- Dessart L, Hillier DJ, Blondin S and Khokhlov A (2014), Apr. [Co III] versus Na I D in Type Ia supernova spectra. *MNRAS* 439: 3114–3120. doi:10.1093/mnras/stu174. 1310.7750.
- Dimitriadis G, Foley RJ, Rest A, Kasen D, Piro AL and et al. (2019), Jan. K2 Observations of SN 2018oh Reveal a Two-component Rising Light Curve for a Type Ia Supernova. *ApJL* 870 (1), L1. doi:10.3847/2041-8213/aadbd0. 1811.10061.
- Dong S, Katz B, Kushnir D and Prieto JL (2015), Nov. Type Ia supernovae with bimodal explosions are common - possible smoking gun for direct collisions of white dwarfs. *MNRAS* 454: L61–L65. doi:10.1093/mnras/slv129. 1401.3347.
- Dwarkadas VV (2024), Jul. X-ray Observations of Two Type Ia Supernovae with an H α Line in their Optical Spectrum. *MNRAS* doi:10.1093/mnras/stae1628. 2407.00279.
- Dwek E (2016), Jul. Iron: A Key Element for Understanding the Origin and Evolution of Interstellar Dust. *ApJ* 825 (2), 136. doi:10.3847/0004-637X/825/2/136. 1605.01957.
- Filippenko AV, Richmond MW, Branch D, Gaskell M, Herbst W and et al. (1992), Oct. The subluminal, spectroscopically peculiar type IA supernova 1991bg in the elliptical galaxy NGC 4374. *AJ* 104: 1543–1556. doi:10.1086/116339.
- Fink M, Röpke FK, Hillebrandt W, Seitzzahl IR, Sim SA and Kromer M (2010), May. Double-detonation sub-Chandrasekhar supernovae: can minimum helium shell masses detonate the core? *A&A* 514, A53. doi:10.1051/0004-6361/200913892. 1002.2173.
- Firth RE, Sullivan M, Gal-Yam A, Howell DA, Maguire K and et al. (2015), Feb. The rising light curves of Type Ia supernovae. *MNRAS* 446 (4): 3895–3910. doi:10.1093/mnras/stu2314. 1411.1064.
- Flörs A, Spyromilio J, Taubenberger S, Blondin S, Cartier R, Leibundgut B, Dessart L, Dhawan S and Hillebrandt W (2020), Jan. Sub-Chandrasekhar progenitors favoured for Type Ia supernovae: evidence from late-time spectroscopy. *MNRAS* 491 (2): 2902–2918. doi:10.1093/mnras/stz3013. 1909.11055.
- Ganeshalingam M, Li W, Filippenko AV, Silverman JM, Chornock R and et al. (2012), Feb. The Low-Velocity, Rapidly Fading Type Ia Supernova 2002es. *ArXiv:1202.3140 [astro-ph.CO]* 1202.3140.
- Geier S, Nesslering S, Heber U, Przybilla N, Napiwotzki R and Kudritzki RP (2007), Mar. The hot subdwarf B + white dwarf binary KPD 1930+2752. A supernova type Ia progenitor candidate. *A&A* 464 (1): 299–307. doi:10.1051/0004-6361:20066098. astro-ph/0609742.
- Hamuy M, Phillips MM, Suntzeff NB, Maza J, González LE and et al. (2003), Aug. An asymptotic-giant-branch star in the progenitor system of a type Ia supernova. *Nature* 424: 651–654. arXiv:astro-ph/0306270.
- Hicken M, Challis P, Jha S, Kirshner RP, Matheson T and et al. (2009), Jul. CfA3: 185 Type Ia Supernova Light Curves from the CfA. *ApJ* 700: 331–357. doi:10.1088/0004-637X/700/1/331. 0901.4787.
- Höflich P (2006), Oct. Physics of type Ia supernovae. *Nucl. Phys. A* 777: 579–600. doi:10.1016/j.nuclphysa.2004.12.038.
- Horowitz CJ and Caplan ME (2021), Apr. Actinide Crystallization and Fission Reactions in Cooling White Dwarf Stars. *Phys. Rev. Lett.* 126 (13), 131101. doi:10.1103/PhysRevLett.126.131101. 2103.02122.
- Hounsell R, Scolnic D, Foley RJ, Kessler R, Miranda V and et al. (2018), Nov. Simulations of the WFIRST Supernova Survey and Forecasts of Cosmological Constraints. *ApJ* 867 (1), 23. doi:10.3847/1538-4357/aac08b. 1702.01747.
- Hoyle F and Fowler WA (1960), Nov. Nucleosynthesis in Supernovae. *ApJ* 132: 565–+.
- Iben Jr. I and Tutukov AV (1984), Feb. Supernovae of type I as end products of the evolution of binaries with components of moderate initial mass (M not greater than about 9 solar masses). *ApJS* 54: 335–372. doi:10.1086/190932.
- Jeffery DJ (1999), Jul. Radioactive Decay Energy Deposition in Supernovae and the Exponential/Quasi-Exponential Behavior of Late-Time Supernova Light Curves. *ArXiv:9907015 astro-ph/9907015*.
- Jha SW (2017), Type Iax Supernovae. Alsabti AW and Murdin P, (Eds.), *Handbook of Supernovae*, pp. 375.
- Justham S (2011), Apr. Single-degenerate Type Ia Supernovae Without Hydrogen Contamination. *ApJL* 730, L34. doi:10.1088/2041-8205/730/2/L34. 1102.4913.
- Kasen D (2010), Jan. Seeing the Collision of a Supernova with Its Companion Star. *ApJ* 708: 1025–1031. doi:10.1088/0004-637X/708/2/1025. 0909.0275.
- Kasen D and Woosley SE (2007), Feb. On the Origin of the Type Ia Supernova Width-Luminosity Relation. *ApJ* 656: 661–665. doi:10.1086/510375. arXiv:astro-ph/0609540.
- Kasen D, Nugent P, Wang L, Howell DA, Wheeler JC and et al. (2003), Aug. Analysis of the Flux and Polarization Spectra of the Type Ia Supernova SN 2001el: Exploring the Geometry of the High-Velocity Ejecta. *ApJ* 593: 788–808. doi:10.1086/376601. arXiv:astro-ph/0301312.
- Kashi A and Soker N (2011), Oct. A circumbinary disc in the final stages of common envelope and the core-degenerate scenario for Type Ia supernovae. *MNRAS* 417 (2): 1466–1479. doi:10.1111/j.1365-2966.2011.19361.x. 1105.5698.
- Kashyap R, Fisher R, García-Berro E, Aznar-Siguán G, Ji S and Lorén-Aguilar P (2015), Feb. Spiral Instability Can Drive Thermonuclear Explosions in Binary White Dwarf Mergers. *ApJL* 800 (1), L7. doi:10.1088/2041-8205/800/1/L7. 1501.05645.
- Katz B and Dong S (2012), Nov. The rate of WD-WD head-on collisions may be as high as the SNe Ia rate. *arXiv e-prints*,

- arXiv:1211.4584[1211.4584].
- Katz B, Kushnir D and Dong S (2013), Jan. An exact integral relation between the Ni56 mass and the bolometric light curve of a type Ia supernova. *arXiv:1301.6766 [astro-ph]* ArXiv: 1301.6766, <http://arxiv.org/abs/1301.6766>.
- Kepler SO, Kleinman SJ, Nitta A, Koester D, Castanheira BG, Giovannini O, Costa AFM and Althaus L (2007), Mar. White dwarf mass distribution in the SDSS. *MNRAS* 375: 1315–1324. doi:10.1111/j.1365-2966.2006.11388.x. astro-ph/0612277.
- Kerzendorf WE, Strampelli G, Shen KJ, Schwab J, Pakmor R, Do T, Buchner J and Rest A (2018), Sep. A search for a surviving companion in SN 1006. *MNRAS* 479 (1): 192–199. doi:10.1093/mnras/sty1357. 1709.06566.
- Khokhlov AM (1991), May. Delayed detonation model for type Ia supernovae. *A&A* 245: 114–128.
- Kool EC, Johansson J, Sollerman J, Moldón J, Moriya TJ and et al. (2023), May. A radio-detected type Ia supernova with helium-rich circumstellar material. *Nature* 617 (7961): 477–482. doi:10.1038/s41586-023-05916-w. 2210.07725.
- Korol V, Buscicchio R, Pakmor R, Morán-Fraile J, Moore CJ and de Mink SE (2024), Jul. Expected insights on type Ia supernovae from LISA's gravitational wave observations. *arXiv e-prints*, arXiv:2407.03935doi:10.48550/arXiv.2407.03935. 2407.03935.
- Kosakowski D, Ugalino MI, Fisher R, Graur O, Bobrick A and Perets HB (2023), Feb. Using ⁴⁴Ti emission to differentiate between thermonuclear supernova progenitors. *MNRAS* 519 (1): L74–L78. doi:10.1093/mnras/slac152. 2210.10804.
- Kromer M, Pakmor R, Taubenberger S, Pignata G, Fink M and et al. (2013), Nov. SN 2010lp—a Type Ia Supernova from a Violent Merger of Two Carbon-Oxygen White Dwarfs. *ApJL* 778 (1), L18. doi:10.1088/2041-8205/778/1/L18. 1311.0310.
- Kromer M, Fremling C, Pakmor R, Taubenberger S, Amanullah R and et al. (2016), Jul. The peculiar Type Ia supernova iPTF14atg: Chandrasekhar-mass explosion or violent merger? *MNRAS* 459 (4): 4428–4439. doi:10.1093/mnras/stw962. 1604.05730.
- Kwok LA, Siebert MR, Johansson J, Jha SW, Blondin S and et al. (2024), May. Ground-based and JWST Observations of SN 2022pul. II. Evidence from Nebular Spectroscopy for a Violent Merger in a Peculiar Type Ia Supernova. *ApJ* 966 (1), 135. doi:10.3847/1538-4357/ad2c0d. 2308.12450.
- Leibundgut B, Kirshner RP, Phillips MM, Wells LA, Suntzeff NB and et al. (1993), Jan. SN 1991bg - A type Ia supernova with a difference. *AJ* 105: 301–313. doi:10.1086/116427.
- Li W, Filippenko AV, Chornock R, Berger E, Berlind P and et al. (2003), Apr. SN 2002cx: The Most Peculiar Known Type Ia Supernova. *PASP* 115: 453–473. arXiv:astro-ph/0301428.
- Lira P, Suntzeff NB, Phillips MM, Hamuy M, Maza J and et al. (1998), Jan. Optical Light Curves of the Type Ia Supernovae SN 1990N and SN 1991T. *AJ* 115 (1): 234–246. doi:10.1086/300175. astro-ph/9709262.
- Maeda K, Taubenberger S, Sollerman J, Mazzali PA, Leloudas G, Nomoto K and Motohara K (2010), Jan. Nebular Spectra and Explosion Asymmetry of Type Ia Supernovae. *ApJ* 708: 1703–1715. doi:10.1088/0004-637X/708/2/1703. 0911.5484.
- Maoz D and Mannucci F (2012), Jan. Type-Ia Supernova Rates and the Progenitor Problem: A Review. *PASA* 29: 447–465. doi:10.1071/AS11052. 1111.4492.
- Maoz D, Mannucci F and Nelemans G (2014), Aug. Observational Clues to the Progenitors of Type Ia Supernovae. *ARA&A* 52: 107–170. doi:10.1146/annurev-astro-082812-141031. 1312.0628.
- Matheson T, Joyce RR, Allen LE, Saha A, Silva DR and et al. (2012), Jul. The Infrared Light Curve of SN 2011fe in M101 and the Distance to M101. *ApJ* 754 (1), 19. doi:10.1088/0004-637X/754/1/19. 1205.3828.
- Mazzali PA, Sullivan M, Hachinger S, Ellis RS, Nugent PE and et al. (2014), Apr. Hubble Space Telescope spectra of the Type Ia supernova SN 2011fe: a tail of low-density, high-velocity material with $Z \lesssim Z_{\odot}$. *MNRAS* 439 (2): 1959–1979. doi:10.1093/mnras/stu077. 1305.2356.
- Nomoto K, Thielemann FK and Yokoi K (1984), Nov. Accreting white dwarf models of Type I supernovae. III - Carbon deflagration supernovae. *ApJ* 286: 644–658. doi:10.1086/162639.
- Nugent P, Phillips M, Baron E, Branch D and Hauschildt P (1995), Dec. Evidence for a Spectroscopic Sequence among Type Ia Supernovae. *ApJL* 455: L147+. doi:10.1086/309846. arXiv:astro-ph/9510004.
- Nugent PE, Sullivan M, Cenko SB, Thomas RC, Kasen D and et al. (2011), Dec. Supernova SN 2011fe from an exploding carbon-oxygen white dwarf star. *Nature* 480: 344–347. doi:10.1038/nature10644. 1110.6201.
- Pakmor R, Kromer M, Röpke FK, Sim SA, Ruiter AJ and Hillebrandt W (2010), Jan. Sub-luminous type Ia supernovae from the mergers of equal-mass white dwarfs with mass $\sim 0.9 M_{\odot}$. *Nature* 463: 61–64. doi:10.1038/nature08642. 0911.0926.
- Pakmor R, Kromer M, Taubenberger S, Sim SA, Röpke FK and Hillebrandt W (2012), Mar. Normal Type Ia Supernovae from Violent Mergers of White Dwarf Binaries. *ApJL* 747, L10. doi:10.1088/2041-8205/747/1/L10. 1201.5123.
- Pakmor R, Kromer M, Taubenberger S and Springel V (2013), Jun. Helium-ignited Violent Mergers as a Unified Model for Normal and Rapidly Declining Type Ia Supernovae. *ApJL* 770, L8. doi:10.1088/2041-8205/770/1/L8. 1302.2913.
- Pakmor R, Callan FP, Collins CE, de Mink SE, Holas A, Kerzendorf WE, Kromer M, Neunteufel PG, O'Brien JT, Röpke FK, Ruiter AJ, Seitzzahl IR, Shingles LJ, Sim SA and Taubenberger S (2022), Dec. On the fate of the secondary white dwarf in double-degenerate double-detonation Type Ia supernovae. *MNRAS* 517 (4): 5260–5271. doi:10.1093/mnras/stac3107. 2203.14990.
- Pakmor R, Seitzzahl IR, Ruiter AJ, Sim SA, Röpke FK, Taubenberger S, Bieri R and Blondin S (2024), Jun. Type Ia supernova explosion models are inherently multidimensional. *A&A* 686, A227. doi:10.1051/0004-6361/202449637. 2402.11010.
- Pelisolì I, Neunteufel P, Geier S, Kupfer T, Heber U and et al. (2021), Jul. A hot subdwarf-white dwarf super-Chandrasekhar candidate supernova Ia progenitor. *Nature Astronomy* 5: 1052–1061. doi:10.1038/s41550-021-01413-0. 2107.09074.
- Pereira R, Thomas RC, Aldering G, Antilogus P, Baltay C and et al. (2013), Jun. Spectrophotometric time series of SN 2011fe from the Nearby Supernova Factory. *A&A* 554, A27. doi:10.1051/0004-6361/201221008. 1302.1292.
- Phillips MM (1993), Aug. The absolute magnitudes of Type Ia supernovae. *ApJL* 413: L105–L108. doi:10.1086/186970.
- Phillips MM, Wells LA, Suntzeff NB, Hamuy M, Leibundgut B, Kirshner RP and Foltz CB (1992), May. SN 1991T: Further Evidence of the Heterogeneous Nature of Type Ia Supernovae. *AJ* 103: 1632. doi:10.1086/116177.
- Phillips MM, Ashall C, Brown PJ, Galbany L, Tucker MA and et al. (2024), Jul. 1991T-like Supernovae. *ApJS* 273 (1), 16. doi:10.3847/1538-4365/ad4f7e. 2405.15027.
- Pierel JDR, Engesser M, Coulter DA, DeCoursey C, Siebert MR and et al. (2024), Aug. Discovery of an Apparent Red, High-velocity Type Ia Supernova at $z = 2.9$ with JWST. *ApJL* 971 (2), L32. doi:10.3847/2041-8213/ad6908. 2406.05089.
- Pinto PA and Eastman RG (2000), Feb. The Physics of Type Ia Supernova Light Curves. II. Opacity and Diffusion. *ApJ* 530: 757–776. doi:10.1086/308380.
- Piro AL and Nakar E (2014), Mar. Constraints on Shallow ⁵⁶Ni from the Early Light Curves of Type Ia Supernovae. *ApJ* 784, 85. doi:10.1088/0004-637X/784/1/85. 1211.6438.
- Poludnenko AY, Chambers J, Ahmed K, Gamezo VN and Taylor BD (2019), Nov. A unified mechanism for unconfined deflagration-to-detonation transition in terrestrial chemical systems and type Ia supernovae. *Science* 366 (6465), aau7365. doi:10.1126/science.aau7365. 1911.00050.
- Prieto JL, Chen P, Dong S, Bose S, Gal-Yam A, Holoién TWS, Kollmeier JA, Phillips MM and Shappee BJ (2020), Feb. Variable H α Emission in the Nebular Spectra of the Low-luminosity Type Ia SN2018cqi/ATLAS18qtd. *ApJ* 889 (2), 100. doi:10.3847/1538-4357/ab6323. 1909.05267.

- Rabinak I, Livne E and Waxman E (2012), Sep. Early Emission from Type Ia Supernovae. *ApJ* 757 (1), 35. doi:10.1088/0004-637X/757/1/35. 1108.5548.
- Richmond MW and Smith HA (2012), Apr. BVRI Photometry of SN 2011fe in M101. *JAAVSO* 40 (2): 872. doi:10.48550/arXiv.1203.4013. 1203.4013.
- Röpke FK (2017), Combustion in Thermonuclear Supernova Explosions, Alsabti AW and Murdin P, (Eds.), Handbook of Supernovae, pp. 1185.
- Rosswog S, Ramirez-Ruiz E and Hix WR (2009), Apr. Tidal Disruption and Ignition of White Dwarfs by Moderately Massive Black Holes. *ApJ* 695 (1): 404–419. doi:10.1088/0004-637X/695/1/404. 0808.2143.
- Scalzo RA, Ruiter AJ and Sim SA (2014), Dec. The ejected mass distribution of Type Ia supernovae: a significant rate of non-Chandrasekhar-mass progenitors. *MNRAS* 445: 2535–2544. doi:10.1093/mnras/stu1808. 1408.6601.
- Seitenzahl IR and Townsley DM (2017), Nucleosynthesis in Thermonuclear Supernovae, Alsabti AW and Murdin P, (Eds.), Handbook of Supernovae, pp. 1955.
- Seitenzahl IR, Cescutti G, Röpke FK, Ruiter AJ and Pakmor R (2013a), Nov. Solar abundance of manganese: a case for near Chandrasekhar-mass Type Ia supernova progenitors. *A&A* 559, L5. doi:10.1051/0004-6361/201322599. 1309.2397.
- Seitenzahl IR, Ciaraldi-Schoolmann F, Röpke FK, Fink M, Hillebrandt W and et al. (2013b), Feb. Three-dimensional delayed-detonation models with nucleosynthesis for Type Ia supernovae. *MNRAS* 429: 1156–1172. doi:10.1093/mnras/sts402. 1211.3015.
- Shen KJ, Bildsten L, Kasen D and Quataert E (2012), Mar. The Long-term Evolution of Double White Dwarf Mergers. *ApJ* 748 (1), 35. doi:10.1088/0004-637X/748/1/35. 1108.4036.
- Shen KJ, Boubert D, Gänsicke BT, Jha SW, Andrews JE and et al. (2018a), Sep. Three Hypervelocity White Dwarfs in Gaia DR2: Evidence for Dynamically Driven Double-degenerate Double-detonation Type Ia Supernovae. *ApJ* 865 (1), 15. doi:10.3847/1538-4357/aad55b. 1804.11163.
- Shen KJ, Kasen D, Miles BJ and Townsley DM (2018b), Feb. Sub-Chandrasekhar-mass White Dwarf Detonations Revisited. *ApJ* 854, 52. doi:10.3847/1538-4357/aaa8de. 1706.01898.
- Stritzinger M, Leibundgut B, Walch S and Contardo G (2006), Apr. Constraints on the progenitor systems of type Ia supernovae. *A&A* 450: 241–251. doi:10.1051/0004-6361:20053652. arXiv:astro-ph/0506415.
- Suyu SH, Huber S, Cañameras R, Kromer M, Schuldt S and et al. (2020), Dec. HOLISMOKES. I. Highly Optimised Lensing Investigations of Supernovae, Microlensing Objects, and Kinematics of Ellipticals and Spirals. *A&A* 644, A162. doi:10.1051/0004-6361/202037757. 2002.08378.
- Taubenberger S (2017), The Extremes of Thermonuclear Supernovae, Alsabti AW and Murdin P, (Eds.), Handbook of Supernovae, pp. 317.
- Taubenberger S, Benetti S, Childress M, Pakmor R, Hachinger S and et al. (2011), Apr. High luminosity, slow ejecta and persistent carbon lines: SN 2009dc challenges thermonuclear explosion scenarios. *MNRAS* 412: 2735–2762. doi:10.1111/j.1365-2966.2010.18107.x. 1011.5665.
- Taubenberger S, Kromer M, Hachinger S, Mazzali PA, Benetti S and et al. (2013), Jul. ‘Super-Chandrasekhar’ Type Ia Supernovae at nebular epochs. *MNRAS* 432 (4): 3117–3130. doi:10.1093/mnras/stt668. 1304.4952.
- Thomas JC, Rodriguez FA, Teitge DS, Kunka LN, Gaddis GN and et al. (2022), Jul. An experimental study of shock transmission from a detonation tube. *Shock Waves* 32 (5): 427–436. doi:10.1007/s00193-022-01086-2.
- Tonry JL, Denneau L, Heinze AN, Stalder B, Smith KW, Smartt SJ, Stubbs CW, Weiland HJ and Rest A (2018), Jun. ATLAS: A High-cadence All-sky Survey System. *PASP* 130 (988): 064505. doi:10.1088/1538-3873/aabadf. 1802.00879.
- Travaglio C, Hillebrandt W, Reinecke M and Thielemann F (2004), Oct. Nucleosynthesis in multi-dimensional SN Ia explosions. *A&A* 425: 1029–1040. doi:10.1051/0004-6361:20041108. arXiv:astro-ph/0406281.
- Tucker MA and Shappee BJ (2024), Feb. The HST Nondetection of SN Ia 2011fe 11.5 yr after Explosion Further Restricts Single-degenerate Progenitor Systems. *ApJ* 962 (1), 74. doi:10.3847/1538-4357/ad1b4e. 2308.08599.
- Tucker MA, Shappee BJ, Kochanek CS, Stanek KZ, Ashall C, Anand GS and Garnavich P (2022), Dec. The whisper of a whimper of a bang: 2400 d of the Type Ia SN 2011fe reveals the decay of ⁵⁵Fe. *MNRAS* 517 (3): 4119–4131. doi:10.1093/mnras/stac2873. 2111.01144.
- Turatto M, Benetti S, Cappellaro E, Danziger IJ, Della Valle M, Gouiffes C, Mazzali PA and Patat F (1996), Nov. The properties of the peculiar type Ia supernova 1991bg. I. Analysis and discussion of two years of observations. *MNRAS* 283: 1–17. arXiv:astro-ph/9605178.
- van Kerkwijk MH, Chang P and Justham S (2010), Oct. Sub-Chandrasekhar White Dwarf Mergers as the Progenitors of Type Ia Supernovae. *ApJL* 722: L157–L161. doi:10.1088/2041-8205/722/2/L157. 1006.4391.
- Webbink RF (1984), Feb. Double white dwarfs as progenitors of R Coronae Borealis stars and Type I supernovae. *ApJ* 277: 355–360. doi:10.1086/161701.
- Wood-Vasey WM, Wang L and Aldering G (2004), Nov. Photometry of SN 2002ic and Implications for the Progenitor Mass-Loss History. *ApJ* 616 (1): 339–345. doi:10.1086/424826. astro-ph/0406191.
- Wygoda N, Elbaz Y and Katz B (2019), Apr. Type Ia supernovae have two physical width-luminosity relations and they favour sub-Chandrasekhar and direct collision models - I. Bolometric. *MNRAS* 484 (3): 3941–3950. doi:10.1093/mnras/stz145. 1711.00969.
- Yoon SC and Langer N (2005), Jun. On the evolution of rapidly rotating massive white dwarfs towards supernovae or collapses. *A&A* 435 (3): 967–985. doi:10.1051/0004-6361:20042542. astro-ph/0502133.